Micromechanical model for isolated polymer-colloid clusters under tension

Roozbeh Dargazany,[1,*] Jiaqi Lin,[2] Leila Khalili,[1] Mikhail Itskov,[3] Hsieh Chen,[2] and Alfredo Alexander-Katz[2]
[1]*Department of Civil and Environmental Engineering, Michigan State University, Michigan 48824, USA*
[2]*Department of Materials Science and Engineering, Massachusetts Institute of Technology, Massachusetts 02139, USA*
[3]*Department of Continuum Mechanics, RWTH Aachen University, 52056 Aachen, Germany*
(Received 27 June 2016; published 10 October 2016)

Binary polymer-colloid (PC) composites form the majority of biological load-bearing materials. Due to the abundance of the polymer and particles, and their simple aggregation process, PC clusters are used broadly by nature to create biomaterials with a variety of functions. However, our understanding of the mechanical features of the clusters and their load transfer mechanism is limited. Our main focus in this paper is the elastic behavior of close-packed PC clusters formed in the presence of polymer linkers. Therefore, a micromechanical model is proposed to predict the constitutive behavior of isolated polymer-colloid clusters under tension. The mechanical response of a cluster is considered to be governed by a backbone chain, which is the stress path that transfers most of the applied load. The developed model can reproduce the mean behavior of the clusters and is not dependent on their local geometry. The model utilizes four geometrical parameters for defining six shape descriptor functions which can affect the geometrical change of the clusters in the course of deformation. The predictions of the model are benchmarked against an extensive set of simulations by coarse-grained-Brownian dynamics, where clusters with different shapes and sizes were considered. The model exhibits good agreement with these simulations, which, besides its relative simplicity, makes the model an excellent add-on module for implementation into multiscale models of nanocomposites.

DOI: 10.1103/PhysRevE.94.042501

I. INTRODUCTION

Colloidal systems represent an attractive class of soft materials whose properties can be tailored by exploiting the individual and collective properties of colloids and their surrounding media. These systems host assemblies of large numbers of colloidal clusters formed by colloids attaching to each other through specific forces or media. While colloidal systems may exhibit different properties at macroscale, their microstructure properties are similar. An important class of colloidal systems is binary polymer-colloid (PC) composites, which consist of two major elements: attractive polymer and nanoparticles. The interactions between colloids in PC clusters are mediated by bridging polymers in a supramolecular fashion. PC clusters exist in a variety of biomaterials. Their assembly yields materials with adjustable properties and a great variation in functionality. However, mechanical properties of these materials have barely been investigated as compared to those of other constituents, such as polymer matrix or particle interface.

Part of this difficulty lies in the complex geometry of these structures and part in their inhomogeneous stress distribution pattern [1,2].

At low particle concentrations, scaling and microstructural models have advanced to describe the rheological [3–5] and mechanical properties [6–8] of PC structures. At high particle concentrations, complicated scaling approaches are developed to account for inelastic features that appear [9,10].

There are two types of load distribution patterns to describe the mechanical response of colloidal systems: (i) wavelike stress distribution in materials such as granular materials, sand piles, and jammed systems [11] and (ii) inhomogeneous pathlike stress distribution in close-packed clusters such as PC clusters [1,2,12]. Generally, due to the fractal nature of PC clusters, when they are subjected to a force, several stress paths are formed inside. One stress path, often the shortest one, transfers the most of the applied load [13]. This stress path is called the backbone chain [5].

In 1990, Shih *et al.* [5] introduced the concept of the effective backbone (BB) chain to explain the stress propagation inside the isolated clusters. Several models have been developed to calculate the energy of the backbone chain [14,15] by representing the chain by a set of thin elastic rods [16] or using the concept of nodes-links-blobs chains [17,18]. Most recent works on the behavior of PC clusters under deformation are numerical studies based on finite-element analysis of accurate substructures [19–23]. Following the concept of the backbone chain, few physically motivated models have been developed to describe the behavior of clusters [6–8], but the underlying changes in the structure of clusters are rarely taken into account. For the moment, to the best of our knowledge, there is no physics-based theory describing the structure-property relation of isolated clusters.

Numerous simulations, experiments, and empirical studies on the mechanics of PC composites have provided us with a good understanding of their behavior at macroscales [10,24,25]. In particular, the mechanical behavior of PC clusters is extensively studied by the rubber community in order to describe the role of silica and carbon black networks on rubber softening during deformation. There are different theories on contribution of clusters to the deformation-induced damage of the matrix, and rubber in particular. Some associate damage to the yielding and reformation of the clusters [26–29], some to gradual softening of the particle-particle bonds [30–32], and some to the changes in cluster sizes and structural rearrangement [33–35]. So far, no consensus on the micromechanics of PC clusters has emerged and, despite its ubiquity and significance, it remains far from understood;

*roozbeh@msu.edu

even the classification of interparticle forces is not agreed on.

While the formation of the backbone chain and stress paths have been shown in several experimental studies [2,36–38], few analytical and simulation studies have investigated the load transfer mechanisms in the aggregates with respect to the stress path formation [23,39–41]. This study mainly focuses on polymer-colloid clusters in which the stress path formation occurs. The process of formation of the backbone chain and its contribution to the mechanics of clusters in different types of aggregation fall has been addressed in a separate study [42].

The mechanical behavior of a cluster is governed by two factors: cluster morphology and the particle interactions. The latter is based on the attraction forces between particles which are mainly induced by polymer chains wrapped around the particles. The attraction forces are categorized into centrosymmetric and tangential forces. Centrosymmetric forces acting along the line that connects centers of the particles to each other are known to play a major role in cluster tensile or compression elasticity [43,44]. Tangential forces acting along the contact surface are known to resist the shear and bending loads; however, our general understanding of them is quite limited [45–47]. While the presence of tangential forces can be inferred from different experiments [48,49], their contribution to the elasticity of clusters is not clear. The backbone chain is considered to be made of several links, where the elongation, bending, and torsion resistance of each bond is mainly derived from the centrosymmetric and tangential forces between the particles. To understand the behavior of clusters, the magnitude of these forces at different places within the cluster should be predicted.

Due to the limited understanding of structural changes in isolated clusters under deformation, micromechanical modeling of the constitute behavior of clusters has remained as a challenging task. So far, the behavior of the clusters is best described by the phenomenological models, which are useful but only relevant in specific cases. Due to the large variety of cluster types, inhomogeneous profiles, and complex structures, the load transfer mechanism in polymer-colloid clusters has not been thoroughly understood and is often excluded or oversimplified in current models. Part of this difficulty lies in correlating the mechanical response of clusters to its structure without getting engaged with its elaborate local topology, part in the complexity of characterization of the clusters geometry, and part in the limitations for coupling of the developed models across different length scales.

To address the concerns, a generalized micromechanical model is developed to describe the averaged behavior of isolated PC clusters in the course of deformation. Accordingly, a two-scale computational-analytical model is presented to describe and validate the mean behavior of clusters regardless of their individual geometry and topology. By excluding the role of local geometry by using shape descriptors, the model can be generalized to all other polymer-colloid clusters aggregated by the attractive forces between polymer and particle surface. In the mesoscale, a micromechanical model is proposed that can calculate the energy of the clusters with respect to four geometrical parameters $\{N,\zeta,d_f,d_b\}$ which are used to represent geometry of clusters. Since the experimental tests on the mechanical behavior of isolated clusters are not available, the results of the model have been compared to Brownian dynamics simulations in microscale. By representing the analytical model in form of a closed-form strain energy equation, the model can be used as a simple add-on module in other multiscale models of PC composites. Such a model can significantly reduce the computational time in concurrent models by replacing the coarse-grain simulations currently use to simulate the behavior of clusters.

This paper is organized as follows. In Section II, the assumptions and simplifications underlying the derivations of the model are discussed. The constitutive formulation of the model is presented in Section III. The derivation of the related shape descriptors and probability functions are discussed in Appendixes A–C. In Section IV, Brownian dynamic simulations are introduced. Several simulations are performed to provide the sample pool required for the verification of the model predictions.

II. GEOMETRY OF THE BACKBONE CHAIN

Considering the backbone chain as an intrinsic part of the cluster, and in view of different deformation states of the backbone chains, we have defined the following three states of deformation:

(1) *Initial unperturbed state (IUS)*: The backbone chain is in a stress-free state, where no external forces are applied. This state is purely hypothetical and does not exists in reality. It is introduced for convenience of mathematical formulation. In view of the polymer models, this state describes the situation where the backbone chain behaves similar to the freely jointed chain.

(2) *Stress-free state (SFS)*: The cluster is in the stress-free state, although the backbone chain is under stress due to the internal forces. The residual force is caused by the adjacent volume filling particles which prevent chain from taking the optimal conformation with respect to the applied load. An illustrative example here is the human body. When no extensional force is applied on the body, the backbone is still under stress due to internal forces forming from the body shape and the gravity.

(3) *Current state*: The cluster and its backbone chain are both subjected to deformation.

Hereafter, IUS will serve as a reference state and will be used to formulate a boundary condition for differential equations governing the evolution of the cluster geometry. The IUS is characterized by the homogeneous spatial distribution of bonds, each of which has the initial length of l, where there is no correlation between their orientations.

Clusters are considered to be fractal at length scales up to ζ and homogeneous at larger length scales. Cluster correlation length ζ [see Fig. 1(a)] is defined as the average distance between two mirrored points on the surface of the cluster in any arbitrary direction [50]. The parameter is calculated when the system is at the SFS.

The correlation length of a backbone chain is related to its number of bonds N as

$$N = \left(\frac{\zeta}{l}\right)^{d_b} = \left(\frac{\zeta}{l}\right)^{1/v}, \tag{1}$$

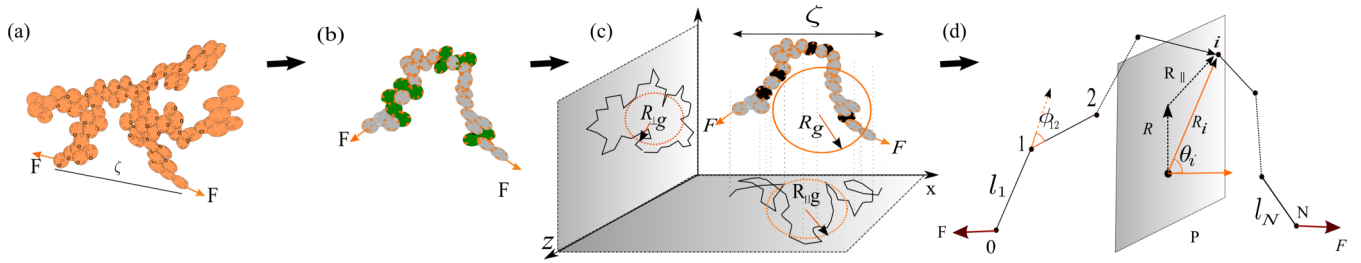

FIG. 1. (a) A schematic view of a cluster subjected to a tensile force. (b) The main stress path; the gray and green particles illustrate the single-particle and multiparticle links, respectively. (c) The radius of gyration of the cluster R_g and the radii of gyration $R_{\perp g}$ and $R_{\parallel g}$ of the projections of the cluster onto planes parallel and normal to the force vector F, respectively. (d) Vectorial representation of a backbone chain with N bonds.

where l is the interpatricle distance, d_b is the fractal dimension of the BB chain [51], and $v = 1/d_b$. In view of the fractal nature of aggregated clusters, d_b is mostly smaller or equal to the fractal dimension of the cluster, d_f. In general, d_f defines the compactness of the cluster and is highly influenced by the aggregation procedure [52]. The lower bound of d_b is 1, corresponding to the straight path of the chain. The upper bound of d_b is $\min[d_f, 5/3]$, where $5/3$ corresponds to the fractal dimension of chains simulated by self-avoiding walk. In Fig. 1(b), a force $\boldsymbol{F}$ is applied on a cluster and the resulting backbone chain is depicted.

With respect to the IUS, the SFS is characterized by a residual stretch, λ_{res} (see Fig. 2). Denoting the applied stretch with respect to SFS by λ_ζ, a (pseudo) stretch λ with respect to the IUS can be defined as

$$\lambda = \lambda_{\text{res}}\lambda_\zeta = \frac{L}{L_0}, \quad L_0^2 = Nl^2, \tag{2}$$

where L_0 and L denote the end-to-end distance of the backbone chain in the IUS and current configuration, respectively.

A vectorial representation of a backbone chain with N bonds is shown in Fig. 1(d) where it is subjected to the volumetric force $\boldsymbol{F}$ (force per unit volume). The interparticle bonds are represented by solidlike beams with identical tensile, bending, and torsion constants. The beam vectors at the IUS configuration are denoted by $\boldsymbol{l}_j$ $(j = 1,2,\ldots,N)$, the cross-sectional area by A_b, and their volume by $V_b = A_b\hat{l}$. The angle between two bonds i and j is represented by $\phi_{i,j}$ and $\hat{\phi}_{i,j}$ in the IUS and current configuration, respectively. In Fig. 1(d), the vector $\boldsymbol{r}_i$ connecting 0th particle to ith particle is expressed by

$$\boldsymbol{r}_i = \sum_{j=1}^{i} \boldsymbol{l}_j. \tag{3}$$

The spatial position, C_G, of the center of gravity of the chain can be defined by the position vector $\boldsymbol{r}_G$ from particle 0 as

$$\boldsymbol{r}_G = \frac{1}{N+1}\sum_{n=1}^{N} \boldsymbol{r}_n. \tag{4}$$

With respect to C_G, the position vector of the ith particle will be denoted by $\boldsymbol{R}_i$. Accordingly, $\|\boldsymbol{r}_N\| = L$ and $\boldsymbol{r}_G = R_0$. The length of a vector $\boldsymbol{x}$ is denoted by $x = \|\boldsymbol{x}\|$. Hereafter, the projection of vector X_i on a plane P normal to the force direction will be represented by X' [see Fig. 1(d)].

The radius of gyration, $R_g = ||R_G||$, is calculated as the mean-square distance of chain particles from the center of gravity, namely

$$R_g^2 = \frac{1}{N+1}\sum_{i=0}^{N} \boldsymbol{R}_i \cdot \boldsymbol{R}_i. \tag{5}$$

The projection of R_G on the reflection plane P is given by $R_{\perp g}$

$$R_{\perp g}^2 = \frac{1}{N+1}\sum_{i=0}^{N} \boldsymbol{R}'_i \cdot \boldsymbol{R}'_i \tag{6}$$

and has significance in describing the topology of clusters. A detailed description on the geometrical parameters introduced here can be found in Refs. [4,15,51,53,54]. The length of a backbone chain, at any stage of deformation, can be then

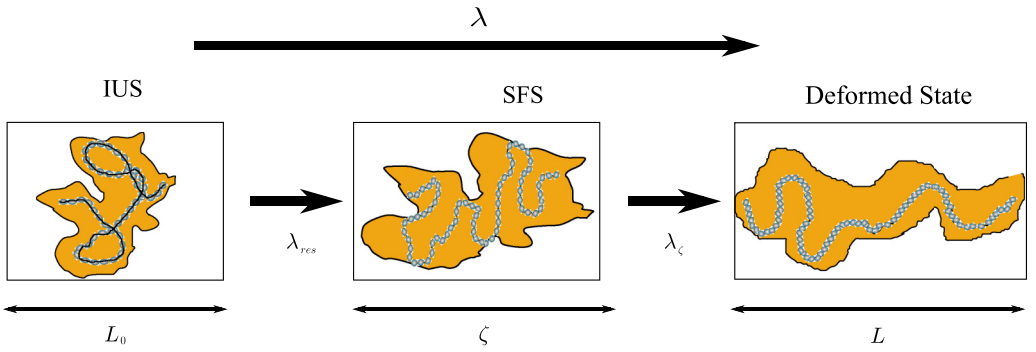

FIG. 2. Conceptual representation of the deformation states and corresponding stretches.

derived from

$$L^2 = \left(\sum_{i=1}^{N} \boldsymbol{l}_i\right) \cdot \left(\sum_{j=1}^{N} \boldsymbol{l}_j\right) = \sum_{i=1}^{N} \boldsymbol{l}_i \cdot \boldsymbol{l}_i + 2\sum_{i=1}^{N-1}\sum_{j=i+1}^{N} \boldsymbol{l}_i \cdot \boldsymbol{l}_j$$
$$= N\bar{l}^2 + 2\bar{l}^2 \sum_{i=1}^{N-1}\sum_{j=i+1}^{N} \cos\phi_{ij}$$
$$= N\bar{l}^2 + N(N-1)\bar{l}^2 b(\lambda). \quad (7)$$

Moreover, in view of Eqs. (2) and (7), one can describe the applied stretch as

$$\lambda^2 = \left(\frac{\bar{l}}{l}\right)^2 [1 + (N-1)b(\lambda)], \quad (8)$$

where $b(\lambda)$ represents the expected value of $\cos\phi_{ij}$ with respect to a random parameter ϕ over all segments distributed in the space, namely

$$b(\lambda) = E[\cos(\phi)]_{\phi}. \quad (9)$$

III. MICROMECHANICAL MODEL

A. Principles and assumptions

The proposed constitutive model is based on the following assumptions:

(1) The backbone chain is considered as the principal source of integrity in the cluster. The contribution of other stress paths is neglected. Thus, the mechanical response of the cluster is assumed to be identical to the response of its backbone chain.

(2) In the backbone chain, more than 60% of all links are single-particle links [1,2]. The multiparticle links have considerable influence on the stability of the backbone chain in compression and prevent further folding and compactification of the cluster. Under tension the multiparticle links act similarly to single-particle links. Accordingly, in this study all the links in the backbone chain are represented by single-particle links.

(3) The model does not consider damage and thus is valid as far as the massive breakage of bonds has not taken place [55]. The bonds are assumed not to be broken or created in the course of deformation.

(4) All particles are assumed to have the same mass and diameter l at IUS. Adjacent particles are assumed to be close enough to each other so the interparticle distance can be approximated by l at the IUS and $\bar{l} > l$ at the current state, respectively.

(5) In the backbone chain, the center of gravity, C_G, is located on the reflection plane P placed in the middle of the end-to-end distance [see Fig. 1(c)].

(6) The stretch applied on the backbone chain is considered to be far smaller than the maximum deformation, $\lambda_{\max}$, in the fully stretched state with $L_{\max} = Nl$. No four consequent particles centers are coplanar.

B. Strain energy

Three types of load are considered to be transferred by the interparticle bonds: tensile-compression force F, bending moment M, and torsion load T. Assuming the bond to behave

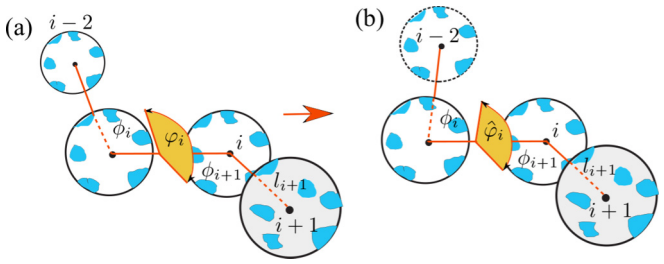

FIG. 3. A four particles strand of the backbone chain under torsion, where the torsion angles in the (a) reference φ_i, and (b) current $\hat{\varphi}_i$ configurations, are shown separately.

elastically in response to these loads, the bond behavior can be represented by three nonlinear elastic springs. Accordingly, following the framework of the Born model [56], the strain energy of a backbone chain in the three-dimensional space is given as the sum of the tensile, bending, and torsional energies by [57–59]

$$\Psi = \underbrace{\frac{G}{2}\sum_{i=1}^{N} \Delta\phi_{i,j}^2}_{\text{Bending}} + \underbrace{\frac{J}{2}\sum_{i=2}^{N} \Delta\varphi_i^2}_{\text{Torsion}} + \underbrace{\frac{Q}{2}\sum_{i=1}^{N} \epsilon_i^2}_{\text{Tension}}, \quad j = i-1, \quad (10)$$

where $\Delta\phi_{i,j} = \hat{\phi}_{i,j} - \phi_{i,j}$ $\Delta\varphi_i = \hat{\varphi}_i - \varphi_i$ $\epsilon_i = 1 - \frac{l_i}{\bar{l}_i}$. Note that $\hat{\boldsymbol{X}}$ represents a reference vector $\boldsymbol{X}$ in current configuration.

Accordingly, $\hat{\varphi}_{i,j}$ and φ_i represents the twist angle of bond i in the current and reference configuration, respectively (see Fig. 3). Q, G, and J denote the averaged linear tensile, bending, and torsion moduli of the bond and are considered to be constant for all the bonds. Such a simplified representation of the elastic moduli of bonds results from the assumption of identical linear springs (ILS), which is adopted here for predicting the energy of the polymer-colloids aggregated clusters. The ILS assumption suggests that all interparticle bonds in an aggregated polymer-colloid cluster can be represented by identical linear springs. If we consider that the behavior of the bonds can be described by three individual nonlinear elastic springs with moduli of $Q_i(x)$, $G_i(\varphi)$, and $J_i(\theta)$, then the ILS assumption is defined as the combination of the following two parts

Part 1: The elastic moduli of bonds is assumed to be linear,

$$Q_i(x) \to Q_i;\ G_i(\varphi) \to G_i;\ J_i(\theta) \to J_i. \quad (11)$$

Part 2: The spring constants of all bonds are assumed identical,

$$Q_i \to Q;\ G_i \to G;\ J_i \to J. \quad (12)$$

The ILS assumption, despite being popular, is an oversimplification of the aggregated structures. It has been rejected by experimental studies in many materials such as disordered fiber networks [60], granular solids, and particulate packings [61]. However, in some materials the error associated to ILS is found to be sufficiently low so it can be adopted [4,5,28,62–67]. Our recent studies show that the ILS assumption is relevant only in

certain binary composites and the error associated to it varies based on the aggregation process [42,68]. While an analysis of the ILS assumption is out of the scope of this paper, our results suggest that the ILS assumption is relevant for close-packed clusters and thus can be used here.

By neglecting the volume of the particles in the lattice, the angle, $\phi_{i,j} \in [0,2\pi]$, is a random variable at the IUS. Accordingly, one can show that $\sum_{i=1}^{N} \Delta\phi_i^2 \approx \sum_{i=1}^{N} \Delta\varphi_i^2$ (see Supplemental Material [69] for calculating the relation between torsion and bending angles). .

The centrosymmetric and tangential forces in three-dimensional settings can be represented by linear elastic elements with an average tensile modulus Q and an average bending-torsion modulus $\bar{G}$. Thus, Eq. (10) is simplified to

$$\Psi = \frac{\bar{G}}{2} \sum_{i=1}^{N-1} \Delta\phi_i{}^2 + Q \sum_{i=1}^{N} \frac{1}{2\hat{l}_i^2} \Delta l_i{}^2, \tag{13}$$

where $\bar{G} = G + J$ while $G = M\Delta\phi_{i,j}^{-1}$ and $J = T\Delta\phi_{i,j}^{-1}$. The strain energy derived in Eq. (13) is the expansion of the two-dimensional (2D) formulation of Ref. [56] into 3D featuring a new function definition for $\bar{G}$.

C. Elastic modulus

By considering the the behavior of a cluster to be described as nonlinear elastic [2,7], its strain energy with respect to the applied force F is given by

$$\Psi = \frac{F^2}{2}\mathcal{H}, \tag{14}$$

where $\mathcal{H}$ is the compliance of the backbone chain. To calculate $\mathcal{H}$, we have to review Eq. (13). Bearing in mind that $\boldsymbol{F}$ represents the volumetric force, the force, and moment balance in bond i (see Fig. 4), it is given by

$$\sigma = Q\epsilon \frac{F V_b \bar{l}_i}{l A_b} \simeq \frac{F l_i \bar{l}_i \cos(\omega_i)}{l} = Q\frac{\Delta l_i}{l},$$
$$\|\boldsymbol{F} V_b \times \boldsymbol{r}_i\| = V_b \bar{G} \Delta\phi_i, \tag{15}$$

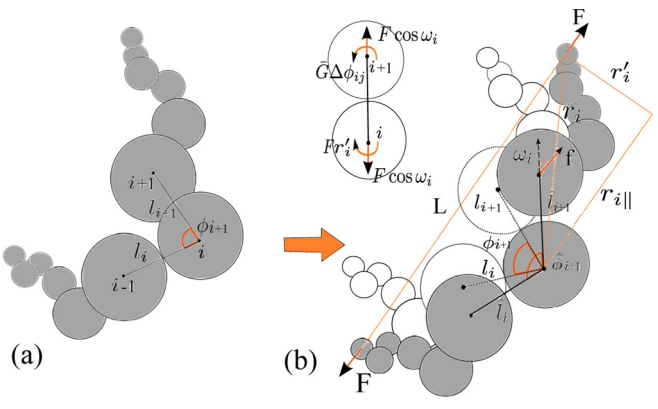

FIG. 4. The (a) reference configuration and (b) current configuration of a backbone chain under bending. Inset: The resultant load balance on bond i.

where ω_i represents the angle between the direction of bond i and the force direction $\boldsymbol{F}$.

Accordingly, the balance equation for one bond gives $Fr'_i = \bar{G}\Delta\phi_i$ and $\Delta l_i = \frac{\hat{l}_i}{Q}\boldsymbol{F}\cdot\boldsymbol{l}_i$ in which

$$\Delta\phi_i = \frac{1}{\bar{G}} \cdot \sum_{j=1}^{i} \boldsymbol{F}\times\boldsymbol{l}_j = \frac{\boldsymbol{F}\times\boldsymbol{z_i}}{\bar{G}} \cdot (\boldsymbol{R}_i - \boldsymbol{R_0}),$$
$$\boldsymbol{R}_i - \boldsymbol{R_0} = \boldsymbol{r}_i. \tag{16}$$

Here, $\boldsymbol{z}_i = \sum_{j=1}^{i} F\boldsymbol{l}_j$ represents the unit vector in the direction of the moment. Inserting Eq. (16) into (13) yields

$$\Psi = \sum_{i=1}^{N} \frac{[(\boldsymbol{F}\times\boldsymbol{z}_i)\cdot\boldsymbol{r}_i]^2}{2\bar{G}} + \frac{1}{2Q}\sum_{i=1}^{N}(\boldsymbol{F}\cdot\boldsymbol{l}_i)^2. \tag{17}$$

Equation (14) gives the compliance of the chain as

$$\mathcal{H} = \left[\frac{L_\perp^2}{\bar{G}} + \frac{L_\parallel^2}{Q}\right], \tag{18}$$

where the parameters $L_\perp$ and $L_\parallel$ represent the normal and parallel relative length of the backbone chain, respectively. Considering $\boldsymbol{R'}_i - \boldsymbol{R'_0} = \boldsymbol{r'}_i$, these parameters will be

$$L_\perp^2 = \sum_{i=1}^{N} \boldsymbol{r'}_i \cdot \boldsymbol{r'}_i = \sum_{i=0}^{N} \boldsymbol{R'}_i \cdot \boldsymbol{R'}_i + (N+1)\boldsymbol{R'}_0 \cdot \boldsymbol{R'}_0$$
$$= (N+1)\left(R_{\perp g}^2 + R_0'^2\right), \tag{19}$$

$$L_\parallel^2 = \sum_{i=1}^{N} (\boldsymbol{f}\cdot\boldsymbol{l}_i)^2 = \sum_{i=1}^{N} (R_i\cos\theta_i - R_{i-1}\cos\theta_{i-1})^2, \tag{20}$$

where $\boldsymbol{f}$ denotes the unit vector of $\boldsymbol{F}$. Here, the 2D model of Kantor and Webman [56] in which $\mathcal{H}$ is a constant has been adopted and modified. The proposed model can consider the deformation-induced structural changes of the cluster with respect to $\mathcal{H}$ and certain shape descriptors as functions of deformation in three dimensions. Accordingly, to the best of our knowledge, the proposed model can express the elasticity moduli of clusters in the case of deformation for the first time.

In view of Eq. (14), we have $\frac{d}{du}(\frac{F^2}{2}\mathcal{H}) = F$. The force and the overall stiffness of the backbone chain K_ζ in the course of deformation are given by

$$F = \frac{1}{\sqrt{\mathcal{H}}}\int_0^u \frac{1}{\sqrt{\mathcal{H}}} du,$$
$$K_\zeta(\lambda) = \frac{F}{u} = \frac{1}{(\lambda-1)\sqrt{\mathcal{H}}}\int_1^\lambda \frac{1}{\sqrt{\mathcal{H}}} d\lambda, \tag{21}$$

where $u = (\lambda - 1)L_0$ is the chain elongation. Such a formulation agrees well with a broad range of experimental observations on the behavior of isolated polymer-colloid clusters. It successfully describes the reduction of the elastic moduli for larger sizes of clusters previously reported by Dinsmore and Weitz [1]. It also takes into account the contribution of bending moments in the behavior of clusters as characterized by Pantina and Furst [7,66,70].

D. Shape descriptors

Using the following averaged trigonometric functions:

$$a(\lambda) = E[R^2 \sin^2\theta]_\theta, \quad b(\lambda) = E[\cos\phi]_\phi,$$
$$c(\lambda) = E[\cos^2\theta]_\theta, \quad d(\lambda) = E[\sin 2\theta]_\theta, \tag{22}$$

the formulations of the shape descriptor functions $L_\perp^2$ and $L_\parallel^2$ given in Eqs. (19) and (20) can be further expanded and simplified to

$$L_\perp^2 \approx N^2 \frac{\bar{l}^2}{12}[1 - b(\lambda)] + Na(\lambda) \tag{23}$$

$$L_\parallel^2 \approx \frac{c(\lambda)l^2}{6}\Bigg(b(\lambda)N^3[1 - c(\lambda)] + 2N^2\left\{[1 - c(\lambda)] - \frac{\pi b(\lambda)d(\lambda)}{4}\right\} - N[\pi d(\lambda) + 2 - 4c(\lambda)]\Bigg). \tag{24}$$

A detailed discussion on the derivation procedure of these formula has been provided in Appendix A.

E. Constitutive model

The constitutive behavior of the backbone chain is derived by implementing Eq. (18) into Eq. (21). Accordingly, K_ζ can be derived as a function of shape descriptors $L_\perp^2$, $L_\parallel^2$, and λ namely as

$$K_\zeta(\lambda) = g(L_\perp^2, L_\parallel^2, \lambda). \tag{25}$$

Substituting $L_\perp^2$ and $L_\parallel^2$ with their expanded formula [derived in Eqs. (A9) and (23) of Appendix B], the stiffness $K_\zeta(\lambda)$ will be derived as a function of deformation which uses four geometrical parameters. The expected value of the aforementioned trigonometric functions [see Eq. (22)] is calculated using

$$E[\Phi(\alpha)]_\alpha = \int_0^\pi \Phi(\tau) P_\alpha(\tau,\lambda) d\tau, \tag{26}$$

where $\Phi(\alpha)$ can be any trigonometric function and α can be either θ or ϕ angles. Accordingly, we have

$$E[\cos\phi]_\phi = \int_0^\pi \cos(\tau) P_\phi(\tau,\lambda) d\tau,$$
$$E[\sin\theta]_\theta = \int_0^\pi \sin(\tau) P_\theta(\tau,\lambda) d\tau. \tag{27}$$

The expected value evolves with deformation due to changes in the angular θ and ϕ distributions. Accordingly, the probability distribution function (PDFs) of the angles θ and ϕ are required for calculation of Eq. (25). The derivation of the PDFs $P_\phi(\phi,\lambda)$ and $P_\theta(\theta,\lambda)$ are discussed in detail in Appendixes B and C, respectively.

To represent the changes of the geometry of a cluster in the course of formulation, the trigonometric functions b, c, and d for a relatively long chain of 100 segments have been calculated and plotted against applied deformation in Fig. 5(a).

IV. VALIDATION

The predictions of the developed model will be benchmarked against tests performed on clusters assembled by the coarse-grained Brownian dynamics simulations.

Since the model provides the mean behavior of clusters, its results will be compared to the average of a large number of simulated clusters.

Three-dimensional PC clusters are assembled by Brownian dynamics simulation [71,72], where the particles are connected to each other through sticking polymer chains (see Fig. 7) [73,74]. The interparticle forces depend mainly on the polymer film between two particles. Such classification can be also considered for other types of colloidal structures, even those without polymer media.

Three major challenges in simulating binary polymer-colloids clusters exist: (i) accurate representation of their structure, (ii) modeling of the aggregation process, and (iii) representation of interparticle forces and moments by spring constants. While the structural properties of clusters can be very complex, studies show that it depends on the aggregation procedure and can be controlled by it [25,72,75]. In this work, PC clusters are assembled with mechanical and structural details close to real clusters, which are formed in shear flow (Fig. 6). After formation, the properties of the clusters are measured outside of the flow.

A. Simulation of clusters by Brownian dynamics

Polymers and colloids are simulated with standard simulating techniques under the framework of the fluctuating lattice Boltzmann (LB) equation [71] in three-dimensional grids with resolutions $N_x \times N_y \times N_z = 64 \times 32 \times 32$. A solid

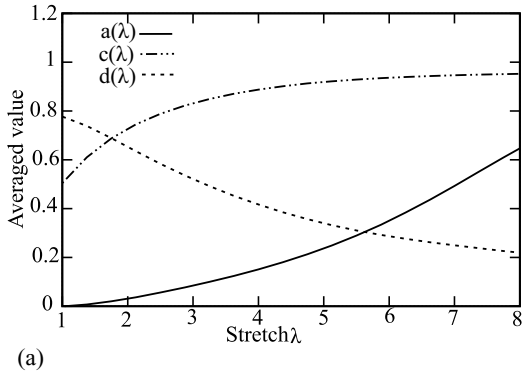

(a)

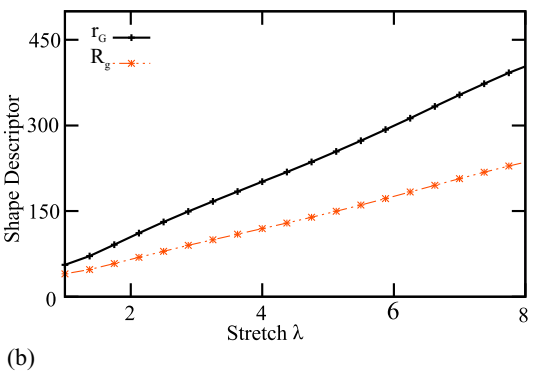

(b)

FIG. 5. (a) Angular functions b, c, and d and (b) the shape descriptor parameters, R_g and r_g of a backbone chain with 100 segments plotted versus stretch.

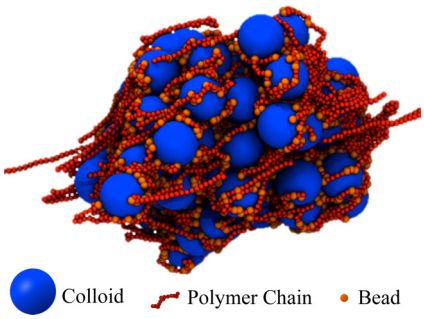

FIG. 6. Representative snapshot of the assembly of an aggregation under strong shear flow.

bounce-back boundary condition is applied in the z direction while the x and y directions are with periodic boundary conditions. The lattice spacing Δx and LB time step Δt are set to unity. The colloids were then simulated using the 'raspberry model" [76,77], where each colloid is made by $N_s = 64$ beads together, forming a spherical shell of diameter $l = 20a$. The shell beads interacted with each other on the same shell through the potential $U_s = (k_s/2)\Sigma_{ij}(d_{ij} - D_{ij})^2$, where d_{ij} and D_{ij} represent the actual and equilibrium distance between beads i and j, respectively [77]. The parameter k_s is an arbitrary spring constant. We used $k_s = 100k_BT/a^2$ to ensure that the colloids will keep their spherical shapes during simulations. The radius of colloids $r_c = 2.5$ and their volume fraction $\phi_c \approx 3\%$. Each polymer consists of $N = 40$ monomers with radius $a = 0.025$ connected with strong springs with a spring constant $k = 1200k_BT/a^2$ and spring length 2a, which renders the polymer freely jointed chain model [74]. Polymers have a volume fraction $\phi_p \approx 0.5\%$. A Lennard-Jones potential is considered for each monomer with strength u to control the solvent properties of the polymers. It has been demonstrated that $u = 0.41$ and $u = 2.08k_BT$ are suitable choices for simulating polymers in the Θ and bad solvent [73,78].

The monomers interact with the colloids at discrete binding sites on the colloid surfaces through the Bell model [79,80], which is a new method to include microscopic associating reactions in highly coarse-grained polymer simulations [see Fig. 7(a)]. In the Bell model, the probability of binding P_B and unbinding P_{UB} reactions are given by

$$P_B = \exp(-E_B/k_BT), \quad P_{\mathrm{UB}} = \exp[-(E_{\mathrm{UB}} - fr_0)/k_BT], \tag{28}$$

where E_B and E_{UB} are the binding and unbinding energy barriers, respectively. Here, f is the average force loaded on the bond, and r_0 is the characteristic bond length which is set $r_0 = 0.01a$ for the simulations. Moreover, k_B is the Boltzmann constant and T the thermodynamic temperature. The binding energy is set to $E_B = 1k_BT$ to ensure fast binding dynamics for bond formation. In order to have a good averaging of the bond force and enough time for the unbinding monomers to diffuse away from its bound partner, the binding and unbinding attempts are performed every 100 LB time steps ($\tau_0 = 100$) [81]. The rest of the parameters for the fluid is as such: the density $\rho = 1$, the kinematic viscosity $\nu = 1/6$, and the relative temperature $k_BT = 5 \times 10^{-5}$. The characteristic monomer diffusion time is $\tau = 6\pi\mu a^3/k_BT \approx 10^3$, where $\mu = \nu\rho$ is the fluid dynamics viscosity.

Figure 7 shows the process of the assembly of a dense aggregate under strong shear flow. In shear flow, the formation of polymer-colloid aggregates is mainly controlled by the competition between the time scales of the polymer unbinding from the colloid versus the rotation or collision time of the colloid. If the polymer unbinding time is significantly longer than the rotation and collision time of the colloid, then the polymers wrap around the colloids and initiate the aggregation process [25,75]. Depending on partial or full wrapping of the polymers on the colloids, the shear-induced aggregates are classified into "no," "loose," "dense," and "log-rolling" aggregates under shear rates $\dot{\gamma}\tau \approx 0.01$ to 0.1, 0.2 to 0.5, 0.6 to 1, and 2, respectively. Here, we focused only on the dense aggregates assembled under shear rate $\dot{\gamma}\tau = 0.8$ with characteristic unbinding energy $E_{\mathrm{UB}} = 6k_BT$ [25,75], in which the colloids are wrapped by the polymers and the film of polymer layer between adjacent particles is the main source of attractive forces between particles.

To measure interparticle forces in a cluster under tension, hydrodynamic interactions are neglected due to their insignificant effects on the mechanical properties of the aggregated clusters under quasistatic tension [77]. Therefore, we implemented only the free draining Brownian dynamics method without LB method for calculation of the elasticity of the interparticle bonds. After mixing interactive colloids and polymers in shear flow, colloids were linked with "sticky" polymers [25]. Permanent links were simulated with stiff springs which are put between monomers and colloid shell beads. Since yielding is not considered here, we set polymer-colloid links nondetachable during the mechanical tests. Therefore, the simulation results cannot be used in large deformation regime where local yielding of the bonds takes place. The dynamics of the ith bead (monomer or colloid shell bead) at position $\boldsymbol{r}_i$ is given by the Langevin

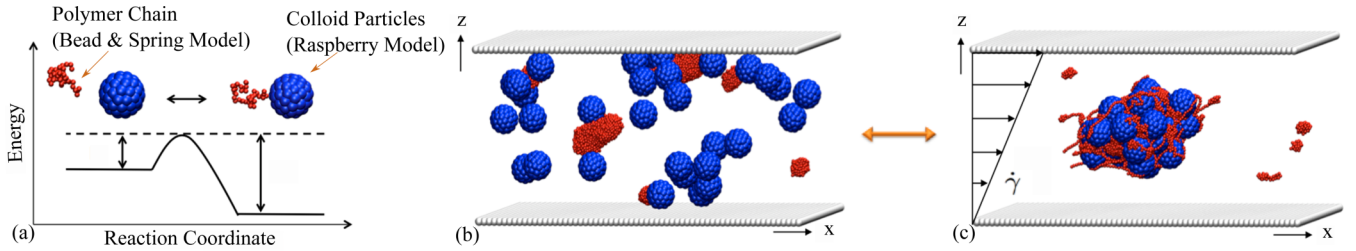

FIG. 7. (a) The bonding mechanism in PC mixtures and representative snapshots of the assembly of a dense aggregate under strong shear flow (b) before and (c) after aggregation.

equation

$$\frac{\partial}{\partial t}\boldsymbol{r}_i = -\mu_0 \bigtriangledown_{\boldsymbol{r}_i} U_i + \xi_i(t), \tag{29}$$

where $\mu_0 = 1/(6\pi\eta_0 a)$ is the Stoke mobility and η_0 the solvent viscosity. The potential energy U_i, which depends on the specific type of the beads (monomer or colloid shell bead), is the summation of all the potentials of bead i. The random force ξ_i satisfies the equation $\langle \xi_i(t)\xi_j(t')\rangle = 2\mu_0 k_B T \Delta_{ij}\Delta(t-t')$. We discretized Eq. (29) with a time step $10^{-4}\tau$, where τ is the characteristic monomer diffusion time $\tau = a^2/\eta_0 k_B T$. Last, to prevent nonphysical penetrations of materials, a harmonic potential was also used between colloids and/or polymers if the distances between their center of masses were smaller than the sum of their radii.

Experimental verification of the simulation. The aggregation model was initially built to analyze the blood clotting process. Special attention has been given to the model with the ability to describe different shapes the clots formed by the shear flow of the media. In our recent studies [42,68], the microscopic structure, connectivity, and bond stiffness have also been validated by comparing the assembled clusters against the results of experimentally confocal microscopy tests performed by Dinsmore *et al.* on PC clusters [1,2]. Moreover, the effective spring constants as of the interparticle bonds can be determined as functions of deformation by measuring the thermal fluctuations of particles in assembled clusters. To validate the simulation results, we have compared the particle fluctuations of the simulated clusters against experimental measurements provided in literature [1,2,12].

B. Benchmarking of the model predictions

The elastic behavior of different isolated PC clusters will be derived from the two sources: the presented model and the simulations. Next, the results are compared with each other. The model predictions are based on the mean conformation of the backbone chain and thus are not influenced by the local geometrical properties of clusters that does not influence any of the parameters $\{N,\zeta,d_f,d_b\}$. Accordingly, the model considers the geometry of two clusters to be identical if their geometrical parameters $\{N,\zeta,d_f,d_b\}$ are identical.

We have previously assembled 16 dense clusters, 5 clusters with $N \approx 32$ particles, 5 with 64, and 3 clusters with N = 96 and 128. Note that the initial structure of the PC cluster is obtained by aggregation in shear flow simulated using the fluctuation lattice-Boltzmann method [72,75]. The mean interparticle elastic moduli Q, G, and J were derived by averaging over the spring moduli of all bonds. While the backbone chain is identified, tracking its changes during deformation is computationally expensive. At this stage, we average over all bonds since we cannot clearly identify and separate those of the backbone chain in the course of deformation. In the next step, the bonds will be categorized based on their connectivity index. Our recent study shows that the bonds with similar connectivity index behave similar whether they are in the backbone chain or not [42]. Interparticle bonds control thermal motions of the particles. By measuring the thermal motions of a bond i, its spring moduli in different Degree of Freedom, namely Q_i, G_i, and J_i are approximated using the equipartition theorem [82]. Excluding thermal noises, these moduli are measured at short time intervals in the course of deformation using the following relations

$$\begin{aligned} Q_i(\langle l_i\rangle)\frac{1}{\langle l_i\rangle^2}\langle l_i - \langle l_i\rangle\rangle^2 &= k_B T, \\ G_i(\langle \phi_{j,ik}\rangle)\langle \phi_{j,ik} - \langle \phi_{j,ik}\rangle\rangle^2 &= k_B T, \\ J_i(\langle \varphi_{ij,kl}\rangle)\langle \varphi_{ij,kl} - \langle \varphi_{ij,kl}\rangle\rangle^2 &= k_B T, \end{aligned} \tag{30}$$

Where <> represents the average value. We previously discussed the process of derivation of the mean elastic moduli of interparticle bonds [68]. Implementing the mean interparticle elastic moduli Q, G, and J along with $\{N,\zeta,d_f,d_b\}$ into the model, the model provides us with $K(\lambda)$ [according to Eq. (25)]. The model presented above includes eight material parameters: three mechanical $\{Q,G,J\}$ and four geometrical ones $\{N,\zeta,d_f,d_b\}$ and A_b. All parameters will be imported from the simulations, except A_b, which is obtained by fitting to the response of one aggregate using the Levenberg-Marquardt algorithm. Here, in Figs. 9 and 10, $A_b = 0.4a^2$ is obtained by fitting of the model predictions against the behavior of the first cluster with 32 particles.

The overall mechanical response of the clusters under applied tension can be divided into three main phases: (i) the elastic phase, (ii) the reformation phase, and (iii) the yield phase. Each phase can be related to the state of the active backbone chain. Phase one illustrates the elastic phase where the backbone chain deforms and orientates towards the load direction. This phase is fully reversible as no permanent change occurs in the backbone chain structure. Phase two is associated with the partial or complete changes of the backbone chain. The changes take place due to the limited extensibility of the former backbone chain. On further deformation, the multiparticle links in the former backbone chain are debonded into several connected single-particle links. This process shortly adds the extensibility limit of the backbone chain; however, once all the soft multiparticles links are debonded, the cluster reaches its maximum extensibility limit and thus enters the next phase. Phase three describes continuous rearrangement and failure of the stress paths during the yielding process where local necking of the end bonds

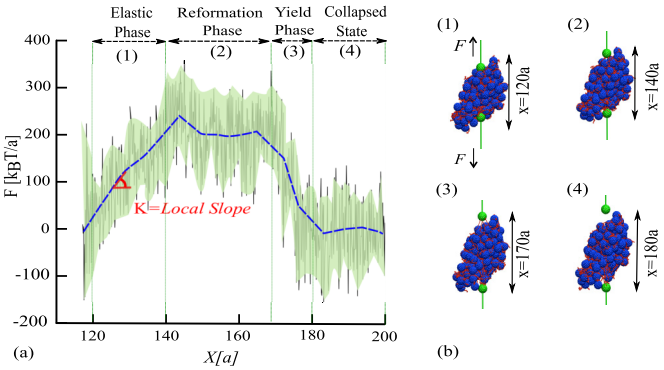

FIG. 8. (a) Representative constitutive behavior of a cluster in the tensile test, and (b) snapshots of the aggregates in the tensile test at each phase. The stages are as follows: (1) initial condition ($X = 120a$), (2) end of elastic phase ($X = 140\,a$), (3) end of reformation phase ($X = 170\,a$), and end of yield phase ($X = 180\,a$).

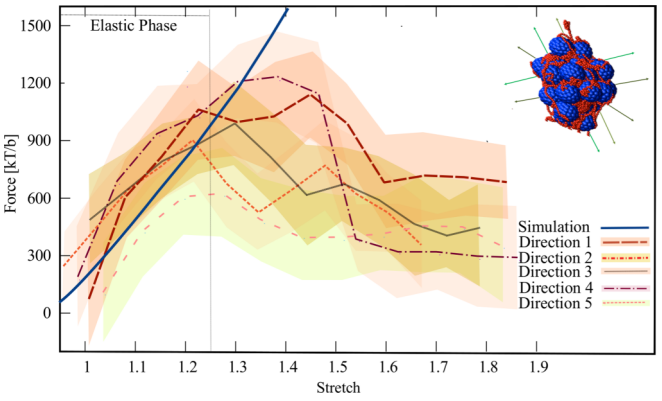

FIG. 9. Force-displacement curves derived from the simulation compared to the predictions of the analytical model for the first aggregate with 32 particles. The mechanical parameters are $Q = 221$, $G = 41$, $J = 47[K_BT/a]$.

happens as illustrated in Fig. 8(4). The proposed model is only relevant in prediction of the elastic phase.

During the yield phase, affine or nonaffine deformation of the clusters has been experimentally observed and reported [67]. The proposed model is only relevant in prediction of the elastic phase. However, the mechanical behavior of the clusters in the yield phase can still be formulated using recent approaches [67] which describe yielding as the decomposition of a cluster into smaller ones. To this end, the strain energy should be calculated as the sum of the energies of the newly formed clusters.

In view of the strong anisotropic geometry of the clusters, each cluster has been subjected to uniaxial tension test at five different directions. These directions are chosen such that the end-to-end distance of the formed backbone chain are similar in all cases. The behavior of a cluster in different directions versus the model predictions has been depicted in Fig. 9.

Using the same geometrical parameters, the model predictions were then compared against the measured response of other four clusters assembled with $N = 32$ particles. Although the local geometry of these clusters differs, their geometrical parameters are almost similar. However, the mechanical parameters differ for each cluster. The good agreement between model predictions and measured values from simulations shown in Fig. 10(a) was obtained automatically.

The error bars here represent the vibration of clusters, not the standard deviation. Their magnitude mainly describe the amplitude of the vibrational expansion and compression of the clusters which results from the Brownian movement of the particles in a small time window. The vibration of the polymers provides the cluster with a beating behavior resembling the one of heart. Thus, tracking the midpoint, peak, or minimum of the vibration curve through deformation will give the same profile. In Figs. 8 and 9 the vibration range is shown by a shaded area. The lower bound depicts the behavior of the minimum value in vibration, the upper bound describes the behavior of the peak, and the solid line represents the mean behavior.

Moreover, the model predictions of the clusters were compared against simulations. As expected from the model, a strong correlation was observed between the elastic behavior of the chain (for $\lambda > 1.3$) and its overall length [see Fig. 10(b)]. No fitting procedure was performed here, and the illustrated agreement is obtained analytically, which shows the predictive capability of the proposed model.

Due to the irregular shape of the cluster, the length of the cluster varies at different directions. The results, however, show that the elastic behavior of the clusters remains almost identical regardless of the loading direction. This fact confirms the relevance of the proposed model, which describes the behavior for a cluster independent of the loading direction. In Fig. 9, the behavior of five clusters, assembled in different shear flows, were compared against the model predictions. Despite the considerable difference between the shape of these clusters, their four shape descriptor parameters $\{N,\zeta,d_f,d_b\}$ were similar and thus their measured behavior were close to each other. Interestingly, the behavior predicted by the model aligns with the simulation results for all cases, which confirms the relevance of the chosen shape descriptor parameters.

The model predicted the mesoscale behavior of PC clusters in elastic regime by representing the interactions resulted from the polymer film around the particles as linear springs [67]. By

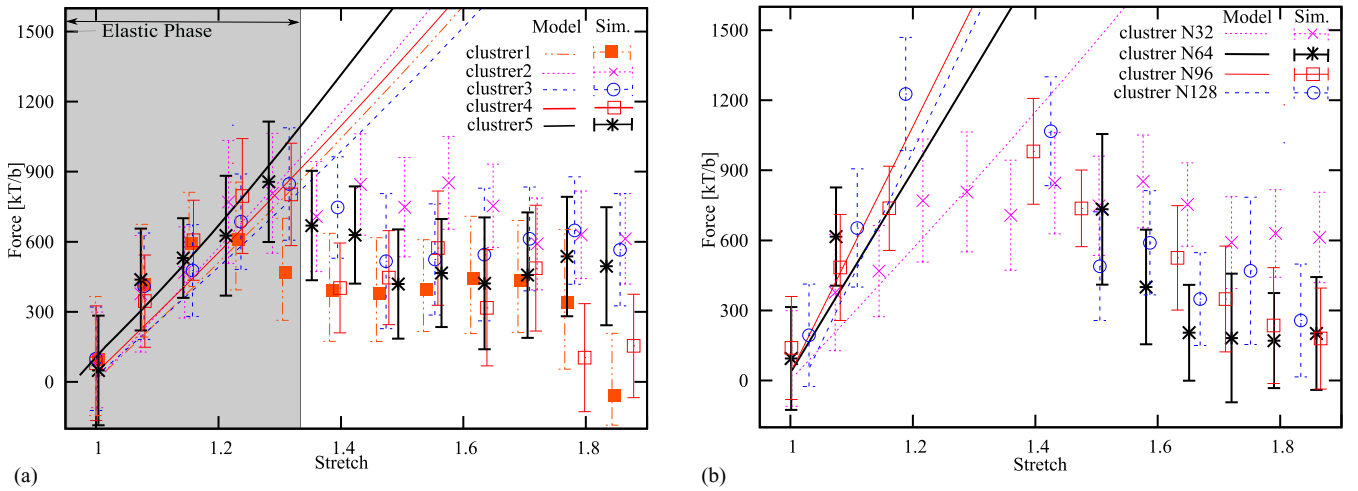

FIG. 10. Force-displacement data measured from coarse-grained Brownian dynamics simulation against the prediction of the proposed model for (a) different clusters with 32 particles and (2) against different sizes of clusters.

adopting the ILS assumption, the model can be used for the clusters with variety of interparticle bonds and interactions. All the material parameters defined in the model are physical and have measurable quantities.

The proposed model is mainly applicable for the dense clusters formed by aggregation of colloids and attractive or nonattractive polymers in shear flow. The load transfer mechanism in these clusters is dominated by the formation of the backbone chain, which is a necessary condition for the proposed model. Such clusters are prevalent in nature and can be found in many binary solutions, ranging from carbon black and silica aggregates in elastomers or thermoplastics to platelets in blood clots to particulate nanocomposites such as polymer bonded explosives. The proposed model is relevant when (i) the temperature is above the glass transition temperature of the matrix, (2) the particle concentration is below the percolation threshold, and (3) only one type of particles exist in the solution.

V. CONCLUSION

The load distribution in the cluster is best described by an entangled network of stress paths, where one stress path transmits most of the load. This path, which is referred to as the backbone chain, governs the response of the whole cluster.

A new micromechanical model is proposed to predict the mechanical behavior of clusters under deformation by describing the response of backbone chains. The model takes into account two sets of geometrical and mechanical parameters. Four geometrical parameters are used to formulate six shape-descriptor parameters to define the changes of the cluster morphology in the course of deformation. The shape descriptors are derived through a generic statistical approach and are as follows: the end-to-end length L [see Eq. (2)], the position vector to the center of gravity r_G [see Eq. (4)], the radius of gyration R_g [see Eq. (5)], the radius of gyration $R_{\perp g}$ of the chain projected to the plane normal to the end-to-end direction [see Eq. (6)], the relative normal length of the chain $L_\perp$ projection on the plane normal to the end-to-end direction [18,56] [see Eq. (19)], and the relative parallel length $L_\parallel$ of the chain projection on the end-to-end direction [see Eq. (20)].

The mechanical behavior of the clusters is formulated in terms of the applied deformation and, consequently, in terms of the four geometrical parameters. Further information on the local geometry of the clusters is provided.

All the material parameters of the model have physical meanings, except A_b; all can be derived experimentally. The model benefits from a simple derivation procedure, low computational costs, and independent of the local geometry, which makes it an excellent choice for multiscale simulations of binary composites. The nonlinear elastic response of different sizes of PC clusters in large deformation can be predicted. Since no direct experimental tests on mechanical behavior of isolated clusters exist, the model predictions have been compared with an extensive set of simulated tests on clusters assembled with Brownian dynamics simulations. In previous studies, the simulation results were validated against several experimental tests. The model predictions show strong agreement with the simulations.

ACKNOWLEDGMENT

This research was supported by the USDOT Tier 1 UTC Center for Highway Pavement Preservation (CHPP) at Michigan State University. The authors are also grateful to MIT MISTI Germany for providing funds for this collaboration. Dr. Alexander-Katz and Dr. Hsieh acknowledge funding from NSF CAREER Award No. DMR-1054671.

APPENDIX A: RELATIVE PARALLEL AND NORMAL LENGTH

1. Relative parallel length

The relative parallel length of a relatively long chain ($\boldsymbol{R}_i \gg \boldsymbol{l}_i$ and $N \gg 1$) is given by

$$L_\parallel^2 = \sum_{i=1}^{N} (R_i \cos\theta_i - R_{i-1}\cos\theta_{i-1})^2, \tag{A1}$$

$$= \sum_{i=1}^{N} {R_i}^2 \cos^2\theta_i + R_{i-1}^2 \cos^2\theta_{i-1} - 2R_i R_{i-1}\cos\theta_i \cos\theta_{i-1}. \tag{A2}$$

It can be shown that for a long chain, $\lim_{N\to\infty} E[\theta_i - \theta_{i-1}]_\theta = 0$. Considering $\Delta = E[\theta_i - \theta_{i-1}]_\theta \approx \frac{\pi}{N}$, one can assume $\sin(\Delta) \approx \Delta$ and $\cos(\Delta) \approx 1$ in case of large N. Accordingly, the last term of Eq. (A2) gives

$$R_i R_{i-1}\cos\theta_i \cos\theta_{i-1} = \frac{\boldsymbol{R}_i \cdot \boldsymbol{R}_{i-1}}{\cos(\Delta)} \cos\theta_i \cos\theta_{i-1}, \tag{A3}$$

where

$$\begin{aligned}\cos\theta_i \cos\theta_{i-1} &= \frac{1}{2}[\cos(\theta_i + \theta_{i-1}) + \cos\Delta] \\ &\approx \frac{1}{2}[\cos(\theta_i + \theta_{i-1}) + 1] \\ &= \frac{1}{2}(\cos 2\theta_i + \Delta \sin 2\theta_i + 1) \\ &\approx \cos^2\theta_i + \frac{\Delta}{2}\sin 2\theta_i\end{aligned} \tag{A4}$$

and

$$\sum_{i=1}^{N} \boldsymbol{R}_i \cdot \boldsymbol{R}_{i-1} = \sum_{i=1}^{N} (\boldsymbol{R}_0 + \boldsymbol{r}_i)\cdot(\boldsymbol{R}_0 + \boldsymbol{r}_{i-1})$$

$$= \sum_{i=1}^{N} R_0^2 + \boldsymbol{R}_0 \cdot \sum_{i=1}^{N} \boldsymbol{r}_i + \boldsymbol{R}_0 \cdot \sum_{i=1}^{N} \boldsymbol{r}_{i-1} + \sum_{i=1}^{N} \boldsymbol{r}_i \cdot \boldsymbol{r}_{i-1}$$

$$= N R_0^2 + 2\boldsymbol{R}_0 \cdot \sum_{i=1}^{N} \boldsymbol{r}_i - \boldsymbol{R}_0 \cdot \boldsymbol{L} + \sum_{n=2}^{N} \left(\sum_{s=1}^{n} \boldsymbol{l}_s \cdot \sum_{t=1}^{n-1} \boldsymbol{l}_t \right)$$

$$= N R_0^2 - 2(N+1) R_0^2 - \boldsymbol{R}_0 \cdot \boldsymbol{L} + \bar{l}^2 \sum_{n=2}^{N} [(n-1) + (n-1)^2 b(\lambda)]$$

$$= -(N+2) R_0^2 + \frac{N\bar{l}^2}{2}\lambda^2 + \frac{\bar{l}^2}{6} N(N-1)[(2N-1)b(\lambda) + 3]. \tag{A5}$$

The radius of gyration given in Eq. (5) can be expanded as

$$R_g^2 = \frac{1}{N+1} \sum_{n=0}^{N} (\boldsymbol{r}_n - \boldsymbol{r}_G) \cdot (\boldsymbol{r}_n - \boldsymbol{r}_G) = \frac{1}{N+1} \sum_{n=0}^{N} \boldsymbol{r}_n \cdot \boldsymbol{r}_n - \boldsymbol{r}_G \cdot \boldsymbol{r}_G. \tag{A6}$$

The first term which is also used in Eq. (7) is given as

$$\sum_{n=1}^{N} \boldsymbol{r}_n \cdot \boldsymbol{r}_n = \sum_{n=1}^{N} \left(\sum_{i=1}^{n} \boldsymbol{l}_i \cdot \sum_{j=1}^{n} \boldsymbol{l}_j \right) = \sum_{n=1}^{N} \left(n\bar{l}^2 + \sum_{\substack{i,j=1 \\ i \neq j}}^{n} \bar{l}^2 \cos\phi_{ij} \right)$$

$$= \sum_{n=1}^{N} \bar{l}^2 [n + n(n-1)b(\lambda)] = \frac{\bar{l}^2}{6} N(N+1)[2b(\lambda)(N-1)+3]. \tag{A7}$$

Here, although the expected value $b(\lambda)$ of the parameter λ is calculated in terms of small number of bonds n, the error is negligible as long as $\sqrt{n} >> 1$. This is a common assumption in the classical perturbation theories [83,84]. Studies on the influence of the bond correlation on the chain end-to-end distance showed that this average scheme yields satisfactory results, even for short chains as well [85]. In view of Eqs. (A13) and (A7), the radius of gyration given in Eq. (A6) takes the form

$$R_g^2 = \frac{\bar{l}^2}{12} \frac{N(N+2)}{(N+1)} [(N-1)b(\lambda) + 2] \approx \frac{N\bar{l}^2}{12} [Nb(\lambda) + 2], \tag{A8}$$

which coincides with the predictions of the linear models [18,84].

Accordingly, the relative parallel length given in view of Eq. (A2) is formulated as

$$L_\parallel^2 = \sum_{i=1}^{N} \left({R_i}^2 \cos^2\theta_i + R_{i-1}^2 \cos^2\theta_{i-1} - 2R_i R_{i-1} \cos\theta_i \cos\theta_{i-1} \right)$$

$$= c\left(2(N+1)R_g^2 - 2R_0^2\right) - (2c + \Delta d) \sum_{i=1}^{N} \boldsymbol{R}_i \cdot \boldsymbol{R}_{i-1}$$

$$\approx \frac{c\bar{l}^2}{6} \left\{ N^2(N-1) \left[(1-c) - \frac{\pi d}{2N} \right] b + 4(N+1)\left(c - \frac{1}{2} \right) + (2-N)\pi d + 2N^2(1-c) \right\}. \tag{A9}$$

2. Relative normal length

The relative normal length is formulated with respect to the parameters $R_{\perp g}^2$ and ${R'_0}^2$ [see Eq. (19)]. The projection of the radius of gyration $R_{\perp g}^2$ can be written by using (6) as

$$(N+1)R_{\perp g}^2 = \sum_{i=0}^{N} \boldsymbol{R'}_i \cdot \boldsymbol{R'}_i = \sum_{i=0}^{N} (\boldsymbol{R}_i \sin\theta_i) \cdot (\boldsymbol{R}_i \sin\theta_i)$$

$$= (N+1)\, a(\lambda), \tag{A10}$$

where $a(\lambda) = E[R^2 \sin^2\theta]_\theta$ represents the expected average of the geometrical parameter $R_i^2 \sin^2\theta_i$ with respect to random parameter θ. The second term of Eq. (A10) can be calculated by Eq. (19), using the following decomposition:

$${R'_0}^2 = {R_0}^2 - {R_{\parallel 0}}^2, \tag{A11}$$

where $\boldsymbol{R}_{\parallel 0}$ is the projection of the position vector of the first particle along the force direction. The parameter $R_0^2 = r_G$ can be derived from Eq. (4) as

$$(N+1)^2 r_G^2 = \sum_{i=1}^{N} \sum_{j=1}^{N} \boldsymbol{r}_i \cdot \boldsymbol{r}_j = \sum_{i=1}^{N} \boldsymbol{r}_i \cdot \boldsymbol{r}_i + 2 \sum_{i=1}^{N-1} \sum_{j=i+1}^{N} \left(\sum_{s=1}^{i} \boldsymbol{l}_s \cdot \sum_{t=1}^{j} \boldsymbol{l}_t \right)$$

$$= \sum_{i=1}^{N} \boldsymbol{r}_i \cdot \boldsymbol{r}_i + 2\bar{l}^2 \sum_{i=1}^{N-1} \sum_{j=i+1}^{N} (i + i(j-1)b)$$

$$= \sum_{i=1}^{N} \boldsymbol{r}_i \cdot \boldsymbol{r}_i + \frac{\bar{l}^2}{12} N(N-1)(N+1) \times [(3N-2)b + 4]. \tag{A12}$$

The first term can be further simplified [as discussed in Eq. (A7)] and rewritten as

$$r_G^2 = \frac{\bar{l}^2}{12}\frac{N}{(N+1)}\left[\left(3N^2 - N - 2\right)b + 4N + 2\right]. \quad \text{(A13)}$$

Moreover, considering the length of the chain in the IUS given by Eq. (2), the parameter $\boldsymbol{R}_{\|0}$ can be expressed in terms of the stretch λ as $R_{\|0}^2 = \frac{1}{4}\lambda^2 N l^2$. Simplifying this equation with respect to Eq. (8) gives

$$R_0'^2 = \bar{l}^2\frac{N(N-1)(1-b)}{12(N+1)}. \quad \text{(A14)}$$

Inserting this expression along with Eqs. (A13) into (19) gives the relative normal length as

$$\begin{aligned} L_\perp^2 &= (N+1)a(\lambda) + \bar{l}^2\frac{N(N-1)[1-b(\lambda)]}{12} \\ &\approx N^2\frac{\bar{l}^2}{12}[1-b(\lambda)] + Na(\lambda). \end{aligned} \quad \text{(A15)}$$

APPENDIX B: PDF OF INTERPARTICLE ANGLES

The PDF of the angle ϕ evolves in the course of deformation. To describe this evolution, two stages of deformation are considered where the profile of the PDF is known: (i) the bell shape distribution at the IUS $\lambda = 1$ and (ii) the Dirac δ profile at the fully stretched state $\lambda = \lambda_{\max}$ with peak at $\phi = 0$ where all the bonds are completely aligned.

To approximate the PDF $P_\phi(\phi,\lambda)$ that can describe both of these profiles, we consider the following Γ distribution function:

$$f(x|\alpha,\beta) = \frac{\beta^\alpha}{\Gamma(\alpha)}x^{\alpha-1}e^{-\beta x}, \quad \text{(B1)}$$

where $\Gamma(\alpha)$ denotes the Γ function [86]. The parameters α and β are both functions of λ and N. Under tension, the bond vectors $\boldsymbol{l}_i$ gradually align with the force direction [see Eq. (3)] so the angles ϕ_{ij} between these vectors tend to zero. The mean value of the distribution function $\mu_\phi(\lambda,N) = \frac{\alpha}{\beta}$ varies with the applied deformation as shown in Eq. (12)(a). Random distribution of bond directions at the IUS and the complete alignment of bond in the force direction at the maximum deformation $\lambda_{\max}$ imply that

$$E[\cos(\phi)]_\phi|_{\lambda=\lambda_{\max}} = 0 \quad \Rightarrow \quad \mu_\phi(1,N) = \frac{\pi}{2}, \quad \text{(B2)}$$

$$E[\cos(\phi)]_\phi|_{\lambda=\lambda_{\max}} = 1 \quad \Rightarrow \quad \mu_\phi(\lambda_{\max},N) = 0, \quad \text{(B3)}$$

where $\lambda_{\max} = \frac{l_{\max}}{l}\sqrt{N}$. Considering $\phi \in [0,\pi]$, normalization of the density Γ distribution Eq. (B1) to this range gives

$$P_\phi(\phi,\lambda) = g_\phi(\lambda)[f(\phi|\alpha(\lambda),\beta(\lambda)) + f(\pi-\phi|\gamma(\lambda),\beta(\lambda))], \quad \text{(B4)}$$

where g_ϕ is a normalization function to ensure $\int_0^\pi P_\phi(\phi,\lambda)d\phi = 1$. An additional condition on the distribution function P_ϕ is applied by Eq. (7). Indeed, inserting Eq. (B4) into Eq. (8) yields

$$\lambda^2 = \left(\frac{\bar{l}}{l}\right)^2\left[1 + (N-1)\int_0^\pi P_\phi(\phi,\lambda)\cos(\phi)d\phi\right], \quad \text{(B5)}$$

TABLE I. Numerical values of the parameters in Eq. (B7)

i	p_i	q_i	r_i	s_i	t_i	$p_{\gamma,i}$	$q_{\gamma,i}$
1	0.008	2.589	0.0007	2.385	0.509	169.2	6.057
2	0.954	0.0856	0.030	−0.870	0.921	23.37	−0.168

which can be used in order to evaluate the PDF of $\alpha(\lambda)$, $\beta(\lambda)$, and $\gamma(\lambda)$. Note that any other type of distribution function can be used here as long as it satisfies Eqs. (B2) and (B5). The Γ distribution here is chosen due to its ability in describing eccentric peaks in distribution of ϕ. The assumed PDF is consistent with the simulation results and describes the boundary conditions quite well [see Fig. 12(b)]. The choice of PDF here can be optimized for clusters with different morphologies, e.g., ultradense clusters with a wavelike stress propagation mechanism. Derivation of the analytical solution of Eq. (B5) is very difficult because of the complexity of the mathematical representation of $(\frac{\bar{l}}{l})^2$. Here, by using the least-squares method, the residual of Eq. (B5) is calculated by

$$\mathcal{R} = \left(\frac{l}{\bar{l}}\right)^2 - \frac{1}{\lambda^2}\left[1 + (N-1)\int_0^\pi P_\phi(\phi,\lambda)\cos(\phi)d\phi\right]. \quad \text{(B6)}$$

Next, the stationary of the residual $\Pi = \int_1^{\lambda_{\max}}\mathcal{R}^2 d\lambda$ is calculated over a class of test functions defined by

$$\alpha \approx \hat{\alpha} = \sum_i p_i(\lambda_{\max}-\lambda)^{q_i}, \quad \gamma \approx \hat{\gamma} = \sum_i p_{\gamma,i}\left(\frac{\lambda}{\lambda_{\max}}\right)^{q_{\gamma,i}},$$

$$\beta \approx \hat{\beta} = \sum_i r_i\lambda^{s_i}(N-1)^{t_i}, \quad \text{(B7)}$$

where $\hat{\alpha}$, $\hat{\beta}$, and $\hat{\gamma}$ represent the approximate solutions of the α, β, and γ that can satisfy Eq. (B5). Their magnitude can be derived from the boundary conditions of the distribution, namely

(i) the sharpness of the PDF at the pole described by $\frac{\alpha}{\beta^2}$ such that $\lim_{N\to 0}\frac{\alpha}{\beta^2} = \infty$,

(ii) the distribution function flattens where the number of bonds tends to infinity,

(iii)at the IUS, the bond vectors are completely uncorrelated, so we have

$$P_\phi(\phi,1) = \tfrac{1}{2}\sin\phi. \quad \text{(B8)}$$

(iv) In the fully stretched state, all the bond vectors are aligned and thus $\phi_{ij} = 0$. Hence,

$$P_\phi(\phi,\lambda_{\max}) = \delta(\phi|0), \quad \text{(B9)}$$

where δ denotes the Kronecker δ. The residual function [Eq. (B6)] are minimized with respect to variables p_i, q_i, r_i, s_i, $p_{\gamma,i}$, $q_{\gamma,i}$ and t_i $(i = 1,2)$ using of the Levenberg-Marquardt algorithm. The calculated values for a backbone chain of 100 particles are given in Table I and the estimated distributed function $P_\phi(\phi,\lambda)$ is plotted in Fig. 11(b) against ϕ for different values of λ.

In Fig. 11(a), the calculated changes in the chain end-to-end distance given in Eq. (B5) is plotted against λ for different clusters sizes based on the values given in Table I. The plot

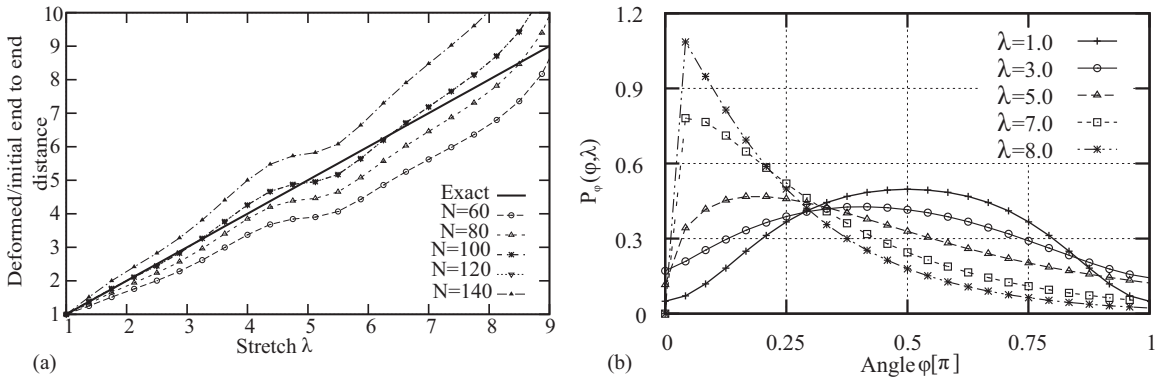

FIG. 11. (a) Square root of the right-hand side of Eq. (B5) plotted versus λ for clusters with different lengths. (b) Interparticle angular distribution of P_ϕ plotted for different stretch levels. The movement of the peak toward zero angle with increasing stretch implies gradual alignment at larger deformations.

illustrates the accuracy of the approximated functions. In the vicinity of the fully stretched state, the error become stronger as more terms of the series α, β, and γ [Eq. (B7)] are required. However, backbone chains are ruptured far before reaching their theoretical fully stretched state. For this reason, the error will not become critical in the range of validity of model which is the elastic phase.

1. Deformation of interparticle bonds

The length of the backbone chain in the deformed configuration is given by

$$L = \sum_{i=1}^{N} (\bar{l}\cos\omega_i) = N\bar{l}E[\cos\omega]_\omega, \tag{B10}$$

which in view of the Eq. (2) yields $\frac{l}{\bar{l}} = \frac{\sqrt{N}}{E}[\cos\omega]_\omega$. By implementing this result into Eq. (B5), we have

$$\frac{l}{\bar{l}} = 1 - \frac{\bar{G}}{Q}(E[\phi]_{\phi|\lambda=1} - E[\hat{\phi}]_\phi)\left(\bar{l}E\left[\frac{1}{r'}\right]_\theta\right)E[\cos\omega]_\omega, \tag{B11}$$

where the variables ϕ_{ij} and r_i' are independent of each other. $\hat{\phi}$ and ϕ are weakly correlated since their interaction is defined by the random parameter ω_i. The magnitudes of $E[\phi]_{\phi|\lambda=1}$ and $E[\hat{\phi}]_\phi$ are obtained from Eq. (26) and plotted in Fig. 12(b) against λ. The mean value of $E[\frac{1}{r'}]_\theta$ will then be obtained by using the PDF of θ through specific procedure described in Appendix D. Considering the symmetric distribution of ω around $\omega = 0$ at different stages of deformation, one has $E[\cos\omega]_\omega = 1$. Consequently, Eq. (B11) yields

$$\frac{l}{\bar{l}} = \frac{\sqrt{N}}{\sqrt{N} + \frac{\bar{G}}{Q}\lambda\bar{l}(E[\phi]_{\phi|\lambda=1} - E[\hat{\phi}]_\phi)E\left[\frac{1}{r'}\right]_\theta}, \tag{B12}$$

which can be inserted in Eq. (B5) in order to calculate b.

APPENDIX C: PDF OF ANGLES OF POSITION VECTORS

The PDF $P_\theta(\theta,\lambda)$ of the angle θ is formulated through discretization of the sample space of the backbone chain which defines the minimum space volume that host all possible conformations of the backbone chain.

Consider a backbone chain with an end-to-end distance L and a contour length $L_C = N\bar{l}$, the sample space is represented by the ellipsoid shown in Fig. 13. The ellipsoid represents all the possible positions of the particles of the backbone chain in space.

The center of gravity C_G of the backbone chain lies on the reflection plane P with an approximate offset R_N' from the end-to-end connecting line. Now, by representing the volume of the solid angle at angle θ by dV_θ (the dark gray zone in

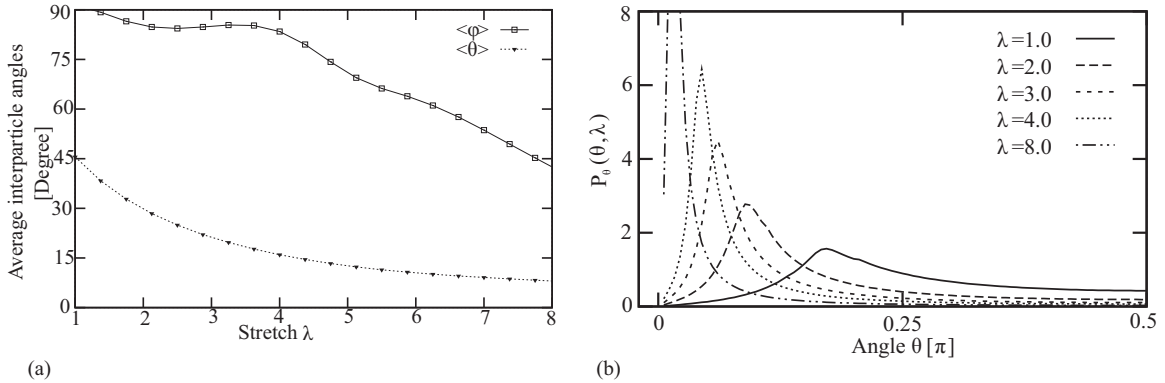

FIG. 12. (a) Mean values of the bond angles $E\langle\phi_{ij}\rangle$ and $E\langle\theta\rangle$ plotted versus stretch. Note that at $\lambda = \lambda_{max}$, the values of both these parameters become zero. (b) The angular distribution of the position vectors $P_\theta(\theta,\lambda)$ at different stretch levels.

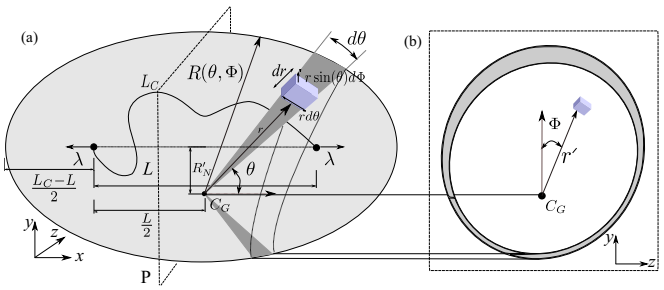

FIG. 13. (a) The ellipsoid representing possible positions of the backbone chain particles. The dark gray zone illustrates a cone element of all particles positioned between the angles θ and $\theta + d\theta$. (b) The front view of the cone element $d\theta$.

Fig. 13), the PDF of θ can be formulated as

$$P_\theta(\theta,\lambda)d\theta = \frac{dV_\theta}{V_{\text{ell}}}, \tag{C1}$$

where $V_{\text{ell}} = \int_0^\pi dV_\theta$ is the sample space and represents the volume of the ellipsoid. Here, the value of dV_θ is defined based on integration of two parameters: (i) the volume of the infinitesimal element $dV_{r\theta\Phi}$ and (ii) $P_p(r,\theta,\Phi)$, which denotes the probability of existence of a chain particle at $dV_{r\theta\Phi}$. Accordingly,

$$dV_\theta = d\theta \int_0^{2\pi}\int_0^{R(\theta,\Phi)} r^2 \sin\theta P_p(r,\theta,\Phi)dr\,d\Phi, \tag{C2}$$

where $P_p(r,\theta,\Phi)$ denotes the probability of existence of a particle at a particular position defined by the coordinates r, θ, and Φ (see Appendix C). Here, $R(\theta,\Phi)$ denotes the outer radius of the ellipsoid at the angles θ and Φ).

1. Cross-sectional averaging

The expected value of trigonometric functions can be derived by implementing Eq. (C1) into Eq. (26). The procedure should be altered for calculation of $E[\frac{1}{r'}]_\theta$ represented in Eq. (B12), since it requires an averaging of the $\frac{1}{r'}$ over projected probability space.

An accurate estimate of upper and lower bounds of $E[\frac{1}{r'}]_\theta$ can hardly be obtained using statistical approaches. Here, the mean values of $\frac{1}{\bar{r}'} = \frac{\bar{l}}{r'}$ are calculated by deriving the value of $\langle\frac{1}{\bar{r}'}\rangle_\theta$ at different cross-sectional planes of the ellipsoid sample space and then averaging it over the whole ellipsoid [see Fig. 13(b)]. The average of $\frac{1}{r'}$ in a cross-sectional plane P_θ of the ellipsoid is expressed by

$$\left\langle\frac{1}{\bar{r}'}\right\rangle_\theta = \frac{\bar{l}^2}{A_\theta}\int_0^{2\pi}\int_0^{\bar{R}(\theta,\Phi)\sin\theta}\left(\frac{1}{r'}\right)r' P_p(r,\theta,\Phi)dr'd\Phi,$$

$$A_\theta = \int_0^{2\pi}\int_0^{R(\theta,\Phi)\sin\theta} r' P_p(r,\theta,\Phi)dr'd\Phi, \tag{C3}$$

where A_θ is the area of the cross-sectional plane P_θ and $r' = r\sin\theta$. Then, one can obtain the mean value $\langle\frac{1}{\bar{r}'}\rangle_\theta$ over the whole ellipsoid by

$$E\left[\frac{1}{r'}\right]_\theta = \int_0^\pi \left\langle\frac{1}{\bar{r}'}\right\rangle_\theta A_\theta \bar{R}(\theta,0)\cos\theta d\theta. \tag{C4}$$

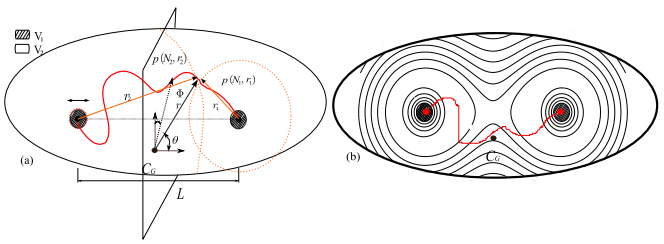

FIG. 14. (a) Dividing the backbone chain into two ideal chains to formulate the probability of a particle in space and (b) schematical view of this probability.

2. PDF of backbone chain particles

Here, we calculate $P_p(r,\theta,\Phi)$, which denotes the probability of existence of a particle of chain at $dV_{r\theta\Phi}$ [see Eq. (C2)]. In the IUS state, the probability density of the nth particle to be at distance between r and $r + dr$ from the 0th segment is

$$P_{\text{seg}}(n,\bar{r})d\bar{r} = \frac{4}{\sqrt{\pi}}B^3\bar{r}^2 e^{-B^2\bar{r}^2}d\bar{r}, \quad \text{where}$$

$$P_{\text{seg}}(n,\bar{r}) = 0\forall\, n < \bar{r} \quad \text{and} \quad B = \sqrt{\frac{3}{2n}}. \tag{C5}$$

Implementing this equation to all the particles of the chain, the probability of finding a particle at the spherical shell of radius r and thickness dr with the origin at particle 0 is given by

$$P_{\text{sh}}(N,\bar{r})d\bar{r} = \frac{1}{N}\sum_{n=1}^{N} P(n,\bar{r})d\bar{r} = \frac{A}{N}\bar{r}^2\sum_{n=1}^{N}(ne^{\frac{\bar{r}^2}{n}})^{-\frac{3}{2}}$$

$$\simeq \frac{A}{N}\int_{n=\bar{r}}^{N}(ne^{\frac{\bar{r}^2}{n}})^{-\frac{3}{2}}dn, \quad \text{where} \quad A = 3\bar{r}^2\sqrt{\frac{6}{\pi}}. \tag{C6}$$

Accordingly, the PDF of existence of a particle at an infinitesimal element $dV_{r\theta\Phi}$ is given by $P_a(N,\bar{r})d\bar{r}$ as

$$P_a(N,\bar{r})d\bar{r} = \frac{P_{\text{sh}}(N,\bar{r})dr}{4\pi\bar{r}^2}$$

$$= \frac{3}{2\pi N\bar{r}}\left[\text{erf}\left(\sqrt{\frac{3\bar{r}}{2}}\right) - \text{erf}\left(\sqrt{\frac{3\bar{r}^2}{2N}}\right)\right]d\bar{r}$$

$$\forall r > 0. \tag{C7}$$

Since the position of the needs of the chain is known, let us divide the backbone chain in the IUS into two chains with N_1 and N_2 segments which are connected to each other by their last links. The probability of the connecting particle to be at a particular position is given by $P_a(N_1,\bar{r}_1)P_a(N_2,\bar{r}_2)$, where $\bar{r}_1 = \frac{r_1}{\bar{l}}$ and $\bar{r}_2 = \frac{r_2}{\bar{l}}$ denote the normalized distances of the particle from each ends of the chain. Since the positions of the first and the last particles are known and their volume is considered nonzero, the total sample space V is divided into two following regions:

(1) V_1: the space occupied by the first and last particles at the ends of the BB chain- hatched area in Fig. 14. Two particles exist in this region.

(2) V_2: the volume of the ellipsoid excluding V1; the plain area in Fig. 14. $N-1$ of $N+1$ particles exist in this region.

Moreover, we know $P_p(r,\theta,\Phi)$ satisfies the following conditions:

$$\int_V P_p(r,\theta,\Phi)dV = 1,$$
$$\int_{V_1} P_p(r,\theta,\Phi)dV = \frac{2}{N+1},$$
$$\int_{V_2} P_p(r,\theta,\Phi)dV = \frac{N-1}{N+1}. \quad \text{(C8)}$$

Since V_1 is fully occupied by the end particles, $P_p(r,\theta,\Phi)$ has a constant value there. Thus, one can write

$$P_p(r,\theta,\Phi) = \begin{cases} \frac{2}{N+1}\frac{3}{8}\frac{1}{\pi l^3} & V_1 \\ \frac{N-1}{N+1}\frac{1}{g_p}p_a(N_1,\bar{r}_1)p_a(N_2,\bar{r}_2) & V_2 \end{cases}, \quad \text{(C9)}$$

where

$$g_p = \int_{V_2} p_a(N_1,\bar{r}_1)p_a(N_2,\bar{r}_2)dV \quad \text{(C10)}$$

is the term normalizing $P_a(N_1,\bar{r}_1)P_a(N_2,\bar{r}_2)$ in V_2. The parameters r_1 and r_2 can be derived from

$$r_1{}^2 = r^2 + R'_0{}^2 + R_{\|0}^2 - 2rR'_0\sin\theta\cos\Phi - 2rR_{\|0}\cos\theta, \quad \text{(C11)}$$

where N_1 and N_2 represent the estimated numbers of segments that connect the particle in consideration with the ends of the backbone chain as shown in Fig. 14. The entropic force of a chain with N segments and the normalized end-to-end distance $\bar{r}$ is written by $F(\bar{r},N) = g(\frac{\bar{r}}{N})$ (see, e.g., Ref. [87]). Since the entropic forces at both parts of the backbone chain are identical, one has $\frac{\bar{r}_1}{N_1} = \frac{\bar{r}_2}{N_2}$. Keeping in mind that the number of segments of the backbone chain with $N+1$ particles is $N_1 + N_2 = N$, one can further write

$$N_1 = N\frac{\bar{r}_1}{\bar{r}_1+\bar{r}_2}, \quad N_2 = N\frac{\bar{r}_2}{\bar{r}_1+\bar{r}_2}. \quad \text{(C12)}$$

[1] A. Dinsmore and D. A. Weitz, Direct imaging of three-dimensional structure and topology of colloidal gels, J. Phys.: Condens. Matter **14**, 7581 (2002).

[2] A. D. Dinsmore, V. Prasad, I. Y. Wong, and D. A. Weitz, Microscopic Structure and Elasticity of Weakly Aggregated Colloidal Gels, Phys. Rev. Lett. **96**, 185502 (2006).

[3] M. H. Lee and E. M. Furst, Response of a colloidal gel to a microscopic oscillatory strain, Phys. Rev. E **77**, 041408 (2008).

[4] W. Y. Shih, W.-H. Shih, and I. A. Aksay, Elastic and yield behavior of strongly flocculated colloids, J. Am. Ceram. Soc. **82**, 616 (1999).

[5] W. H. Shih, W. Y. Shih, S. I. Kim, J. Liu, and I. A. Aksay, Scaling behavior of the elastic properties of colloidal gels, Phys. Rev. A **42**, 4772 (1990).

[6] R. Dargazany and M. Itskov, Yield behavior of colloidal aggregates due to combined tensile-bending loads, Phys. Rev. E **85**, 051406 (2012).

[7] J. P. Pantina and E. M. Furst, Elasticity and Critical Bending Moment of Model Colloidal Aggregates, Phys. Rev. Lett. **94**, 138301 (2005).

[8] J. Jancar, J. Douglas, F. W. Starr, S. Kumar, P. Cassagnau, A. Lesser, S. S. Sternstein, and M. Buehler, Current issues in research on structure–property relationships in polymer nanocomposites, Polymer **51**, 3321 (2010).

[9] N. Koumakis and G. Petekidis, Two step yielding in attractive colloids: transition from gels to attractive glasses, Soft Matter **7**, 2456 (2011).

[10] C. Storm, J. Pastore, F. MacKintosh, T. Lubensky, and P. Janmey, Nonlinear elasticity in biological gels, Nature **435**, 191 (2005).

[11] C. Goldenberg and I. Goldhirsch, Friction enhances elasticity in granular solids, Nature **435**, 188 (2005).

[12] A. D. Dinsmore, E. R. Weeks, V. Prasad, A. C. Levitt, and D. A. Weitz, Three-dimensional confocal microscopy of colloids, Appl. Opt. **40**, 4152 (2001).

[13] J. Wong, A. K. Gaharwar, D. Mueller-Schulte, D. Bahadur, and W. Richtering, Layer-by-layer assembly of a magnetic nanoparticle shell on a thermoresponsive microgel core, J. Magn. Magn. Mater. **311**, 219 (2007).

[14] J. Geng, D. Howell, E. Longhi, R. P. Behringer, G. Reydellet, L. Vanel, E. Clément, and S. Luding, Footprints in Sand: The Response of a Granular Material to Local Perturbations, Phys. Rev. Lett. **87**, 035506 (2001).

[15] T. Gisler, R. C. Ball, and D. A. Weitz, Strain Hardening of Fractal Colloidal Gels, Phys. Rev. Lett. **82**, 1064 (1999).

[16] A. Potanin, On the computer simulation of the deformation and breakup of colloidal aggregates in shear flow, J. Colloid Interface Sci. **157**, 399 (1993).

[17] C. Lin and Y. Lee, Strain-dependent dynamic properties of filled rubber network systems, 2: The physical meaning of parameters in the l-n-b model and their applicability, Macromolec. Theor. Simul. **6**, 339 (1997).

[18] C. Lin, Y. Chen, and C. Chang, A links-nodes-blobs model for conductive polymer composites, Macromolec. Theor. Simul. **10**, 219 (2001).

[19] D. Sodhani and S. Reese, Finite element-based micromechanical modeling of microstructure morphology in filler-reinforced elastomer, Macromolecules **47**, 3161 (2014).

[20] E. Tarleton, M. Charalambides, and C. Leppard, Image-based modeling of binary composites, Comput. Mater. Sci. **64**, 183 (2012); *Proceedings of the 21st International Workshop on Computational Mechanics of Materials* (IWCMM 21).

[21] Z. Guo, X. Shi, Y. Chen, H. Chen, X. Peng, and P. Harrison, Mechanical modeling of incompressible particle-reinforced neo-hookean composites based on numerical homogenization, Mech. Mater. **70**, 1 (2014).

[22] D. Bray, P. Dittanet, F. Guild, A. Kinloch, K. Masania, R. Pearson, and A. Taylor, The modeling of the toughening of epoxy polymers via silica nanoparticles: The effects of volume fraction and particle size, Polymer **54**, 7022 (2013).

[23] H. Arora, E. Tarleton, J. Li-Mayer, M. Charalambides, and D. Lewis, Modelling the damage and deformation process in a plastic bonded explosive microstructure under tension using the finite element method, Comput. Mater. Sci. **110**, 91 (2015).

[24] P. J. Lu, E. Zaccarelli, F. Ciulla, A. B. Schofield, F. Sciortino, and D. A. Weitz, Gelation of particles with short-range attraction, Nature **453**, 499 (2008).

[25] H. Chen, M. A. Fallah, V. Huck, J. I. Angerer, A. J. Reininger, S. W. Schneider, M. F. Schneider, and A. Alexander-Katz, Blood-clotting-inspired reversible polymer–colloid composite assembly in flow, Nat. Commun. **4**, 1333 (2013).

[26] H. Lorenz, D. Steinhauser, and M. Klppel, Morphology and micro-mechanics of filled elastomer blends: Impact on dynamic crack propagation," in *Fracture Mechanics and Statistical Mechanics of Reinforced Elastomeric Blends*, edited by W. Grellmann, G. Heinrich, M. Kaliske, M. Klppel, K. Schneider, and T. Vilgis, Vol. 70 of Lecture Notes in Applied and Computational Mechanics (Springer, Berlin, Heidelberg, 2013), pp. 81–128.

[27] H. Lorenz and M. Klüppel, Microstructure-based modeling of arbitrary deformation histories of filler-reinforced elastomers, J. Mech. Phys. Solids **60**, 1842 (2012).

[28] J. Meier and M. Klüppel, Carbon black networking in elastomers monitored by dynamic mechanical and dielectric spectroscopy, Macromolec. Mater. Eng. **293**, 12 (2008).

[29] M. Klüppel, The role of disorder in filler reinforcement of elastomers on various length scales, Adv. Polym. Sci. **164**, 1 (2003).

[30] R. Perez-Aparicio, A. Vieyres, P.-A. Albouy, O. Sanseau, O. au, L. Vanel, D. R. Long, and P. Sotta, Reinforcement in natural rubber elastomer nanocomposites: Breakdown of entropic elasticity, Macromolecules **46**, 8964 (2013).

[31] A. Papon, S. Merabia, L. Guy, F. Lequeux, H. Montes, P. Sotta, and D. R. Long, Unique nonlinear behavior of nano-filled elastomers: From the onset of strain softening to large amplitude shear deformations, Macromolecules **45**, 2891 (2012).

[32] S. Merabia, P. Sotta, and D. R. Long, A microscopic model for the reinforcement and the nonlinear behavior of filled elastomers and thermoplastic elastomers (payne and mullins effects), Macromolecules **41**, 8252 (2008).

[33] R. Dargazany, V. N. Khiêm, U. Navrath, and M. Itskov, Network evolution model of anisotropic stress softening in filled rubber-like materials; parameter identification and finite element implementation, J. Mech. Mater. Struct. **7**, 861 (2013).

[34] R. Dargazany, V. N. Khiêm, and M. Itskov, A generalized network decomposition model for the quasi-static inelastic behavior of filled elastomers, Int. J. Plast. **63**, 94 (2015).

[35] R. Dargazany and M. Itskov, Constitutive modeling of the mullins effect and cyclic stress softening in filled elastomers, Phys. Rev. E **88**, 012602 (2013).

[36] S. Kohjiya, A. Katoh, T. Suda, J. Shimanuki, and Y. Ikeda, Visualisation of carbon black networks in rubbery matrix by skeletonisation of 3d-tem image, Polymer **47**, 3298 (2006).

[37] J. Zhou and A. D. Dinsmore, A statistical model of contacts and forces in random granular media, J. Stat. Mech.: Theor. Exp. (2009) L05001.

[38] J. Zhou, S. Long, Q. Wang, and A. D. Dinsmore, Measurement of forces inside a three-dimensional pile of frictionless droplets, Science **312**, 1631 (2006).

[39] S. Gan, Z. L. Wu, H. Xu, Y. Song, and Q. Zheng, Viscoelastic behaviors of carbon black gel extracted from highly filled natural rubber compounds: Insights into the payne effect, Macromolecules **49**, 1454 (2016).

[40] L. Yang, S. Huang, F. Wu, S. Zheng, W. Yang, Z. Liu, and M. Yang, New insights into the elasticity and multi-level relaxation of filler network with studies on the rheology of isotactic polypropylene/carbon black nanocomposite, RSC Adv. **5**, 65874 (2015).

[41] J. Hager, R. Hentschke, N. W. Hojdis, and H. A. Karimi-Varzaneh, Computer simulation of particle–particle interaction in a model polymer nanocomposite, Macromolecules **48**, 9039 (2015).

[42] R. Dargazany, H. Chen, J. Lin, A. Alexander-Katz, and M. Itskov, On the validity of representation of the inter-particle forces by linear springs in aggregated clusters (unpublished).

[43] G. Foffi, C. De Michele, F. Sciortino, and P. Tartaglia, Scaling of Dynamics with the Range of Interaction in Short-Range Attractive Colloids, Phys. Rev. Lett. **94**, 078301 (2005).

[44] S. Manley, H. M. Wyss, K. Miyazaki, J. C. Conrad, V. Trappe, L. J. Kaufman, D. R. Reichman, and D. A. Weitz, Glasslike Arrest in Spinodal Decomposition as a Route to Colloidal Gelation, Phys. Rev. Lett. **95**, 238302 (2005).

[45] A. West, J. Melrose, and R. Ball, Computer simulations of the breakup of colloid aggregates, Phys. Rev. E **49**, 4237 (1994).

[46] R. Botet and B. Cabane, Scaling behaviors of colloidal aggregates under uniform pressure, Phys. Rev. E **70**, 031403 (2004).

[47] V. Becker and H. Briesen, Tangential-force model for interactions between bonded colloidal particles, Phys. Rev. E **78**, 061404 (2008).

[48] T. Dabroś and T. Van de ven, A direct method for studying particle deposition onto solid surfaces, Colloid Polym. Sci. **261**, 694 (1983).

[49] E. Velegol, S. Catana, J. L. Anderson, and S. Garoff, Tangential Forces Between Nontouching Colloidal Particles, Phys. Rev. Lett. **83**, 1243 (1999).

[50] D. Stauffer and A. Aharony, *Introduction to Percolation Theory*, 2nd ed. (CRC Press, London, 1994).

[51] G. A. Arteca, Scaling behavior of some molecular shape descriptors of polymer chains and protein backbones, Phys. Rev. E **49**, 2417 (1994).

[52] C. Herd, G. Mcdonald, and W. Hess, Morphology of carbon black aggregates: Fractal versus euclidean geometry, Rubber Chem. Technol. **65**, 107 (1992).

[53] C. Liem and N. Jan, Fractal properties of the percolating backbone in three dimensions, J. Phys. A: Math. Gen. **21**, 243 (1988).

[54] D. Laidlaw, G. MacKay, and N. Jan, Some fractal properties of the percolating backbone in two dimensions, J. Stat. Phys. **46**, 507 (1987).

[55] R. Bandyopadhyaya, W. Rong, and S. Friedlander, Dynamics of chain aggregates of carbon nanoparticles in isolation and in polymer films: Implications for nanocomposite materials, Chem. Mater. **16**, 3147 (2004).

[56] Y. Kantor and I. Webman, Elastic Properties of Random Percolating Systems, Phys. Rev. Lett. **52**, 1891 (1984).

[57] S. Arbabi and M. Sahimi, Mechanics of disordered solids. I. percolation on elastic networks with central forces, Phys. Rev. B **47**, 695 (1993).

[58] S. Arbabi and M. Sahimi, Elastic properties of three-dimensional percolation networks with stretching and bond-bending forces, Phys. Rev. B **38**, 7173 (1988).

[59] H. He and M. F. Thrope, Elastic Properties of Glasses, Phys. Rev. Lett. **54**, 2107 (1985).

[60] M. Sheinman, C. P. Broedersz, and F. C. MacKintosh, Actively Stressed Marginal Networks, Phys. Rev. Lett. **109**, 238101 (2012).

[61] M. C. Jenkins, M. D. Haw, G. C. Barker, W. C. K. Poon, and S. U. Egelhaaf, Does Gravity Cause Load-Bearing Bridges in Colloidal and Granular Systems?, Phys. Rev. Lett. **107**, 038302 (2011).

[62] N. Stübler, J. Fritzsche, and M. Klüppel, Mechanical and electrical analysis of carbon black networking in elastomers under strain, Polym. Eng. Sci. **51**, 1206 (2011).

[63] H. Kruggel-Emden, S. Wirtz, and V. Scherer, A study on tangential force laws applicable to the discrete element method (dem) for materials with viscoelastic or plastic behavior, Chem. Eng. Sci. **63**, 1523 (2008).

[64] J. G. Meier, J. W. Mani, and M. Klüppel, Analysis of carbon black networking in elastomers by dielectric spectroscopy, Phys. Rev. B **75**, 054202 (2007).

[65] A. G. Marangoni, Elasticity of high-volume-fraction fractal aggregate networks: A thermodynamic approach, Phys. Rev. B **62**, 13951 (2000).

[66] E. M. Furst and J. P. Pantina, Yielding in colloidal gels due to nonlinear microstructure bending mechanics, Phys. Rev. E **75**, 050402 (2007).

[67] N. Jouault, F. Dalmas, F. Boué, and J. Jestin, Nanoparticles reorganizations in polymer nanocomposites under large deformation, Polymer **55**, 2523 (2014).

[68] R. Dargazany, A. Rege, and M. Itskov, Elasticity of colloidal clusters with application to carbon-black aggregates in filled rubbers, Const. Models Rubber VIII **8**, 261 (2013).

[69] See Supplemental Material at http://link.aps.org/supplemental/10.1103/PhysRevE.94.042501 for information on how to calculate the relation between torsion and bending angles.

[70] J. P. Pantina and E. M. Furst, Micromechanics and contact forces of colloidal aggregates in the presence of surfactants, Langmuir **24**, 1141 (2008).

[71] B. Dünweg and A. J. C. Ladd, Lattice Boltzmann Simulations of Soft Matter Systems, in *Advanced Computer Simulation Approaches for Soft Matter Sciences III*, edited by C. Holm and K. Kremer, Advances in Polymer Science, Vol. 221 (Springer-Verlag, Berlin, Heidelberg, 2009), pp. 89–166.

[72] H. Chen and A. Alexander-Katz, Dynamics of Polymers in Flowing Colloidal Suspensions, Phys. Rev. Lett. **107**, 128301 (2011).

[73] A. Alexander-Katz, M. F. Schneider, S. W. Schneider, A. Wixforth, and R. R. Netz, Shear-Flow-Induced Unfolding of Polymeric Globules, Phys. Rev. Lett. **97**, 138101 (2006).

[74] C. E. Sing and A. Alexander-Katz, Elongational flow induces the unfolding of von willebrand factor at physiological flow rates, Biophys. J. **98**, L35 (2010).

[75] H. Chen and A. Alexander-Katz, Structure and dynamics of blood-clotting-inspired polymer-colloid composites, Soft Matter **9**, 10381 (2013).

[76] V. Lobaskin and B. Dünweg, A new model for simulating colloidal dynamics, New J. Phys. **6**, 54 (2004).

[77] A. Alexander-Katz, Motion-reversal in a simple microscopic swimmer, arXiv:0705.2669 (2007).

[78] A. Alexander-Katz and R. R. Netz, Dynamics and instabilities of collapsed polymers in shear flow, Macromolecules **41**, 3363 (2008).

[79] G. I. Bell, Models for specific adhesion of cells to cells, Science **200**, 618 (1978).

[80] H. Chen and A. Alexander-Katz, Polymer-based catch-bonds, Biophys. J. **100**, 174 (2011).

[81] C. E. Sing and A. Alexander-Katz, Giant Nonmonotonic Stretching Response of a Self-Associating Polymer in Shear Flow, Phys. Rev. Lett. **107**, 198302 (2011).

[82] L. Landau and E. Lifshitz, *Mechanics* (Pergamon, New York, 1976).

[83] M. Fixman, Excluded volume in polymer chains, J. Chem. Phys. **23**, 1656 (1955).

[84] M. Kosmas, On the mean radius of gyration of a polymer chain, J. Phys. A: Math.Gen. **14**, 2779 (1981).

[85] M. Zimmt, K. Peterson, and M. Fayer, Short polymer chain statistics and the relationship to end to end electronic excitation transport: Random walks with variable-step lengths, Macromolecules **21**, 1145 (1988).

[86] R. V. Hogg, A. Craig, and J. McKean, *Introduction to Mathematical Statistics*, 4th ed. (Macmillan, New York, 1978).

[87] R. Dargazany and M. Itskov, A network evolution model for the anisotropic Mullins effect in carbon black filled rubbers, Int. J. Solids Struct. **46**, 2967 (2009).